Major Project Report

by Andrew John Alexander Noble

FILE	3483_ANDREW_JOHN_ALEXANDER_NOBLE_MAJOR_PROJECT_REPORT_128469_1737240490.DOCX (12.58M)		
TIME SUBMITTED	24-APR-2019 12:35PM (UTC+0100)	WORD COUNT	18883
SUBMISSION ID	105250390	CHARACTER COUNT	104748



University of Wales Trinity Saint David

School of Engineering

Major Project Thesis

An Investigation into Flow Management Methods to Control Front Wheel Wake on Open Wheel Race Cars

Andrew Noble

BEng (Hons) Motorsport Engineering

2019

Supervisor: Tim Tudor

Abstract

Investigations are to be conducted into the generation and propagation of front wheel wake in the context of an open wheel, single seat race vehicle. The investigations were carried in using validated Computation Fluid Dynamics. Initially the investigations will focus on the possibility of utilising deformable composite structures for aerodynamic gain, primarily looking at the use of front brake ducts to manipulate flow, although this has ultimately proven unsuccessful.

Further investigations were then conducted, focusing on the use of upstream aerodynamic devices, namely front wings, to manage the wheel wake downstream on a vehicle. The investigation is based around the regulatory changes seen in Formula 1 for the 2019 season, intended to limit outwash. It was found that, while designing within the confines of the 2019 regulations, it is possible to generate similar outwash characteristics to the previous generation designs, which then produced very similar wake structures. The impact of the front wing on the front wheel wake was found to be significant, in terms of the intensity and the direction, to varying extents depending on the design philosophy.

An additional study has been conducted looking at the impact of the vehicle wake, which was found to be heavily influenced by the management of the front wheel wake, on a vehicle driving directly into the wake. Reductions in Cl were found to be between 21% and 16%, while reductions in Cd were between 13% and 4% on the following car.

Declaration of Authenticity

This thesis is the result of the authors original research. It has been composed by the author and has not been previously submitted for examination which has led to the award of a degree.

Signed: Andrew Noble Date: 29/04/2019

Acknowledgments

I would like to thank Tim Tudor for his continued advice and support on the subject matter throughout the duration of the project.

Special mention to Tiegen Lillicrap for her collaborative work in the early stages of the project as well as keeping spirits high throughout. Fellow student John Hughes must be acknowledged for his support and assistance with the ANSYS software and aerodynamic discussions.

Special thanks go to John Iley, of Iley Design, for his welcome interest and valued advice on the direction of the project, as well as insight into wake management techniques in F1.

Contents

Abstract 1

Declaration of Authenticity 1

Acknowledgments 1

1.0 Project Introduction & Relevancy 6

2.0 Project Aims & Timescales 8

2.1 Specific Aims 8

2.2 Supplementary/Time Dependant Aims 8

2.3 Projected Timescales 9

3.0 Literature Review 10

3.1 Understanding Wheel Wake 10

3.2 Brake Cooling Ducts 10

3.3 Computational Fluid Dynamics 12

3.3.1 Reference Geometry 12

3.3.2 Domain Sizing 12

3.3.3 Mesh Size 13

3.3.4 Mesh Density Zones 13

3.3.5 Turbulence Models 14

3.4 CFD Methodology 14

3.5 Design of Experiment 16

3.6 Turbulent Flow & Wake Structures 17

4.0 CFD Validation Study 19

4.1 Design of Experiment Approach 19

4.2 Iterative Validation Study 20

5.0 Brake Duct Investigation 23

5.1 Initial Basic Geometry Testing 23

5.2 Design Iteration Testing 27

5.2.1 Slot Gap Testing 27

5.2.2 Varied Duct Opening Size 32

5.3 Testing Conclusions 34
6.0 Front Wing Design Investigations 38
6.1 Representative Geometries 38
6.2 Wing in Isolation Testing 40
6.3 1/3 Car Model Design Testing 42
6.4 Full Car Geometry Testing 46
6.5 Following Car Testing 55
6.5.1 Wake Profile of Single Vehicle 55
6.5.2 Following Car CFD Testing 59
7.0 Conclusion & Evaluation 64
8.0 Recommended Further Works 66
Works Cited 67
Appendix A 72
A.1 Thermal Management Issues 72
A.2 Simulator Brake Temperature Testing 72

Figure 1 - Project Gannt Chart 9
Figure 2 - Turbulent Wheel Wake (Croner, et al., 2013) 10
Figure 3 - Carbon Braking System Temperature Management (Airbus, 2014) 11
Figure 4 - Ahmed Body Dimensions (CFD Online, 2014) 12
Figure 5 - Navier-Stokes Equations (NASA, 2009) 15
Figure 6 - CFD Workflow (Alahmer & Al-Dabbas, 2014) 16
Figure 7 - Wake Formation Behind Cylindrical Object (Wenjun, et al., 2018) 18
Figure 8 - Box-Benkham Experimental Design 19
Figure 9 - Iterative Validation Study Results 21
Figure 10 - Ahmed Body Vortex Comparison (Guilmineau, et al., 2017) 22
Figure 11 - Dallara GP2/11 Brake Duct (FIA Formula 2, 2017) 23
Figure 12 - Simplistic Brake Duct Testing Geometry 24
Figure 13 - Brake Duct Initial Run Pressure Distribution 24
Figure 14 - Brake Duct Initial Run Velocity Contours 25
Figure 15 - Vorticity Regions Original Geometry 26
Figure 16 - Brake Duct Initial Run Velocity Profile 27
Figure 17 - Slot Gap Testing Positions 28

Figure 18 - Slot Gap Testing Assembly Cl Cd Results 28
Figure 19 - Slot Gap Testing Duct Cl Cd Results 29
Figure 20 - Slot Gap Testing Flow Vectors 29
Figure 21 - Slot Gap Testing Duct Pressures 30
Figure 22 - Slot Gap Testing Turbulent Flow around Duct 31
Figure 23 - Slot Gap Testing Flow Vectors Forward Opening 31
Figure 24 - Duct Opening Size Results on Assembly 32
Figure 25 - Areas of Turbulent Flow around Duct 33
Figure 26 - Duct Opening Size Results on Duct 33
Figure 27 - Brake Duct Opening Tests Pressure Contours 34
Figure 28 - Flow Vectors showing influence of duct flow 35
Figure 29 - Rotating Wheel Wake Comparison Velocity Contours 37
Figure 30 - Rotating F1 Wheel Wake Example (Axereo-Cilies & Iaccarino, 2012) 37
Figure 31 - F1 2018 Wing Geometry (F1Technical.net, 2018) 38
Figure 32 - 2019 Wing Geometry Comparison (FIA Formula 1, 2018) 39
Figure 33 - F1 Car Geometry (Perrinn, 2017) 39
Figure 34 - Representative Wheel and Duct Assembly. Image: (MaxF1.net, 2019) 40
Figure 35 - Wing in Isolation Specification Comparison 40
Figure 36 - Wing in Isolation Streamlines Rear View 41
Figure 37 - Design Concepts 42
Figure 38 - 1/3 Car Testing Results 44
Figure 39 - 2018 Spec Velocity Cut Plane 0.2m from ground 44
Figure 40 - 1/3 Car Testing Wheel Wake Velocity Cut Planes 45
Figure 41 - Pressures on Wing Undersides Designs 1,4,5,7 46
Figure 42 - Full Car Geometry Testing Results 47
Figure 43 - Full Car Geometry Testing Centre of Pressure Results 48
Figure 44 - Full Car Geometry Testing Underside Pressure Distributions 49
Figure 45 - Full Car Geometry Testing Designs 1,4 & 7 Underside Pressures 50
Figure 46 - Full Car Geometry Testing Velocity Cut Plane Designs 1 & 4 51
Figure 47 - Front Wing Upwash Characteristics 51
Figure 48 - Full Car Geometry Testing Turbulent Kinetic Energy Isosurface 52
Figure 49 - Full Car Geometry Testing 2018 Spec Turbulent Kinetic Energy 53
Figure 50 - Velocity Contours Section View 0.35m above Ground Plane 53
Figure 51 - Force India 2018 Front Brake Assembly (FIA Formula 1, 2018) 54
Figure 52 - Y250 Vortex Designs 1 and 7 55
Figure 53 - Vehicle Wake 2.5m behind car designs 1 & 8 55
Figure 54 - Isosurface showing wake region designs 1 & 8 Side View 56

Figure 55 - Isosurface showing wake region designs 1 & 8 Rear view 56
Figure 56 - F1 Car Wake Representation (Newbon, et al., 2017) 57
Figure 57 - Vehicle Wake Differences Plane 0.25m above ground 57
Figure 58 - F1 2018 2019 Wake Comparison (Iley Design, 2019) 58
Figure 59 - Following Car CFD Testing Geometry 2019 Spec Cars 59
Figure 60 - Cl and Cd results from 5 Car Length Separation Testing 59
Figure 61 - Following Car Testing Cl Percentage Values 60
Figure 62 - Following Car Testing Cd Percentage Values 60
Figure 63 - Following Car Testing Velocity Contours 61
Figure 64 - Following Car Cl Results 0.35s Separation 62
Figure 65 - Following Car Cd Results 0.35s Separation 63
Figure 66 - 2019 Specification Following Car Isosurface 63

Table 1 - CFD Standardised Settings 20
Table 2 - DOE Parameters and Ranges 20
Table 3 - Iterative Validation Study Base Settings 21
Table 4 - Duct Opening Dimensions 32
Table 5 - Cl Cd Results of Duct compared to Assembly 36
Table 6 - Design Concept Details 43

1.0 Project Introduction & Relevancy

Within many of the higher tiers of motorsport, the aerodynamics of the vehicle make an incredibly valuable contribution to its overall performance. As such, teams and designers have long been looking to make breakthroughs that push and exploit the regulations that restrict them, to gain a performance advantage.

One of the areas that has been developed, and continues to still be an area of interest, is that of movable aerodynamic devices, to act as variable flow conditioners as well as changing lift and drag properties. Within almost all race series, at any level of competition, fully movable and controllable aerodynamic devices are banned (Motorsport Association, 2018) (Federation International de l'Automobile, 2018), apart from the active Drag Reduction Systems seen in F1, F2 and GP3 (Formula1.com, 2018). The heavy regulation of the area has forced teams to explore options that fall within the interpretation of the rules, resulting in clever use of the prescribed design areas to produce the desired flow structures while still producing a device that delivers in terms of overall aerodynamic efficiency.

The area of mechanical deflection has been explored heavily within the Formula 1 community for at least the last 8 years, with teams still making use of the technology to their advantage, whilst passing the static load tests (Kajiwara, 2017). It should be said that the FIA, and other governing bodies are constantly looking at areas such as these, often attempting to close loopholes and rewrite the rules so that they are not open to interpretation and exploitation. While this area shows promise, the constant constraint from regulatory bodies and complexity in being able to accurately simulate the transient effects with the computational resource available, mean that this project will focus solely on fixed geometry changes.

An area that has already been explored, although seemingly to a lesser extent, is that of inducing deflection in an aerodynamic structure using heat. As such, this project intends to look at the viability of using heat to induce a change in the attitude of a composite structure into the airflow, and therefore the influence that this can have on the aerodynamic performance of a component, a subject touched on by (Yokozeki, 2006). Specifically initial investigations will focus on what can be achieved in the front brake duct area of the vehicle, given that there is a considerable heat source in the vicinity of the device, and the knowledge that front brake ducts have been an area of heavy development for controlling

flow structures around the front wheel in Formula 1 over recent years, as detailed in an article by (Motorsport.com, 2016).

Additionally, focus will be placed on front wing structures, using the Formula 1 style package as a template. This decision is driven by analysis of the considerable literature about front wing interaction and influence on wake structures, clearly showing that this upstream component is one of the most crucial for wake management. Based on the rule changes that are coming into force for the Formula 1 2019 season, which have mandated considerable change to the front wing geometries, with the intent of changing the way teams manage flow structures and vehicle wake as per (FIA Formula 1, 2018), the decision was taken to look specifically at the difference between 2018 designs and the varied options available within the 2019 regulations.

Regarding the validation study that must be conducted for the CFD element of the project, the intent is to approach this in a novel manner. Traditionally, the validation studies are conducted in an iterative manner (Medes-Alves & de Almeaida, 2017), which whilst accurate, are time consuming (Versteeg & Malalasekera, 2007). It is the intent of this project to apply Design of Experiment (DOE) to the validation study to see if the same results can be obtained, whilst minimising the number of steps required to reach the end settings (Field & Hole, 2003). After some research, this approach does not seem to have been documented previously.

2.0 Project Aims & Timescales

2.1 Specific Aims

- Gain a good working understanding of Ansys/Fluent CFD software to be used throughout the project.
- Conduct a validation study using CFD to ensure any future results obtained are accurate and valid, based on the Ahmed Body geometry. Study to be conducted with the use of DOE software, Design Expert 11.
- Identify and create a CAD models of suitably representative geometries, like those found in current Formula 1 designs.
- Investigate and understand the current aerodynamic properties of the wake structure.
- Conduct studies into the differing design options and the associated impact of flow structures.

2.2 Supplementary/Time Dependant Aims

- Produce test pieces and conduct physical testing to validate the simulated data.
- Utilise the wind tunnel facility to help validate the simulated results.
- Select a suitable car model and investigate the influence on the overall aerodynamic performance instead of just on the selected component.

2.3 Projected Timescales

Figure 1 shows the Gannt chart relating to the planned workflow for the project duration.

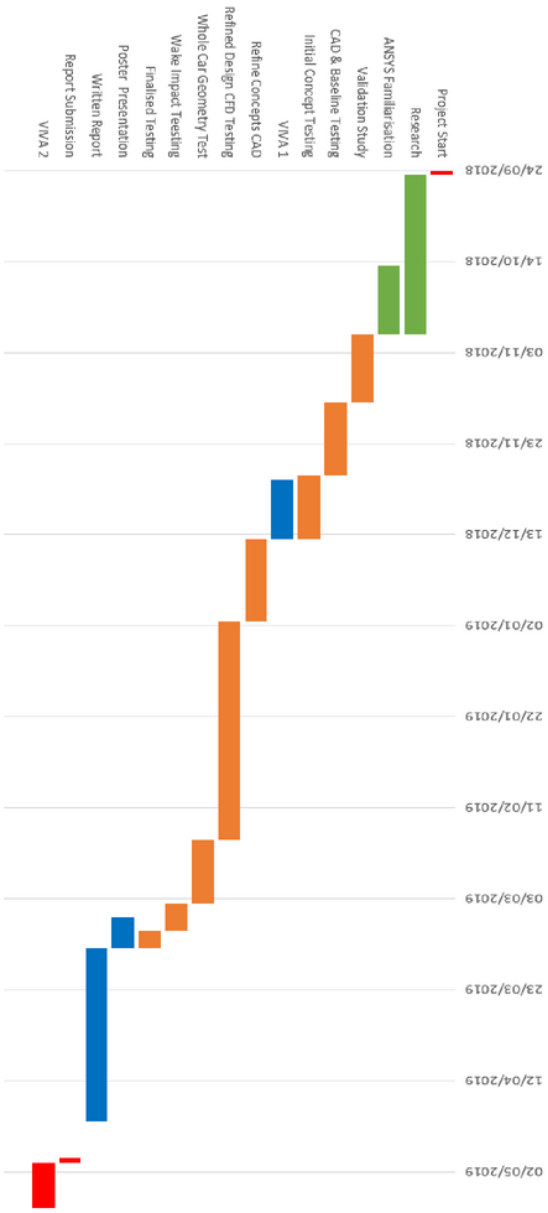


Figure 1 - Project Gannt Chart

3.0 Literature Review

3.1 Understanding Wheel Wake

As detailed by (Saddington, et al., 2007) the phenomenon of aerodynamic wake generated by a rotating wheel in the context of open wheeled race cars is not well understood, especially when it comes to the interaction of the wheel with other aerodynamic devices around it. Given that (Wright, 2001) states the exposed wheels on an F1 car account for around 35% of the total drag of the vehicle, and the impact of the front wheel wake on the downstream components can be significant, it is understandable why considerable effort is currently being employed by designers to understand and manage this wake.

The wheel can be compared to a bluff body moving through an airflow, bounded on its lower surface by the ground plane. Modelling the flow around this type of body statically is not a new concept, however this only tells part of the story when looking at rotating wheels. The works by (Saddington, et al., 2007) (Diasinos, et al., 2015) and (Croner, et al., 2013) have shown the importance of having the wheel rotating, either in a wind tunnel or computational domain. This changes the structure of the wake left behind significantly, with the trailing vortices changing in intensity and position dramatically.
Figure 2 shows a representation of the generated wheel wake from CFD results based on a rotating wheel, showing the considerable wake region.

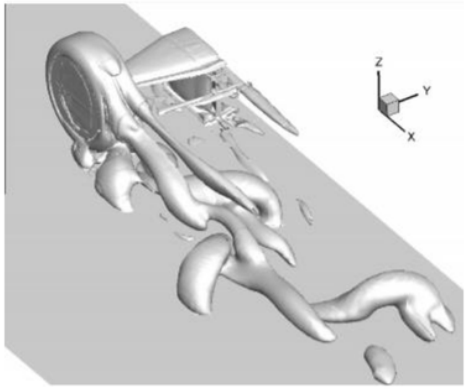


Figure 2 - Turbulent Wheel Wake (Croner, et al., 2013)

3.2 Brake Cooling Ducts

Cooling on a race car is a necessary evil in the eyes of an aerodynamicist. The drivetrain components and brake assemblies require specific levels of cooling to be able to operate without risk of failure, however these cooling orifices inevitably create drag, which slows the vehicle (Smith, 1978). If the cooling opening can be minimised, this can offer a significant

reduction in the vehicles overall drag coefficient, thus resulting in increased lap times. However, consideration must still be given to the cooling requirements of the surrounding components. If a system could be designed that allows for a duct to be designed below the minimum required size, but then expand to create the required geometry to meet the cooling requirements, this could be of significant benefit. Since the regulations across almost all series of motorsport preclude the use of movable aerodynamic devices, it would be necessary to create this geometric change using a composite structure that would not be classed as a “movable aerodynamic device”, thus staying within the letter, if not the spirit of the rules.

One area where there is a clear thermal input is the brake duct. On a single seat vehicle, the duct is attached directly to the hub assembly, thus placing it very close to the heat source of the brake materials. Since the brake systems of a single seat car only require cooling during and immediately after the braking events, there is a strong argument to be made for reducing the drag implication on the assembly when not needed. However, consideration must still be given the thermal management of the braking systems, more information on which can be found in Appendix A, with figure 3 giving an example of the significant temperature variances that can be seen with carbon braking systems, albeit in an aeronautical context.

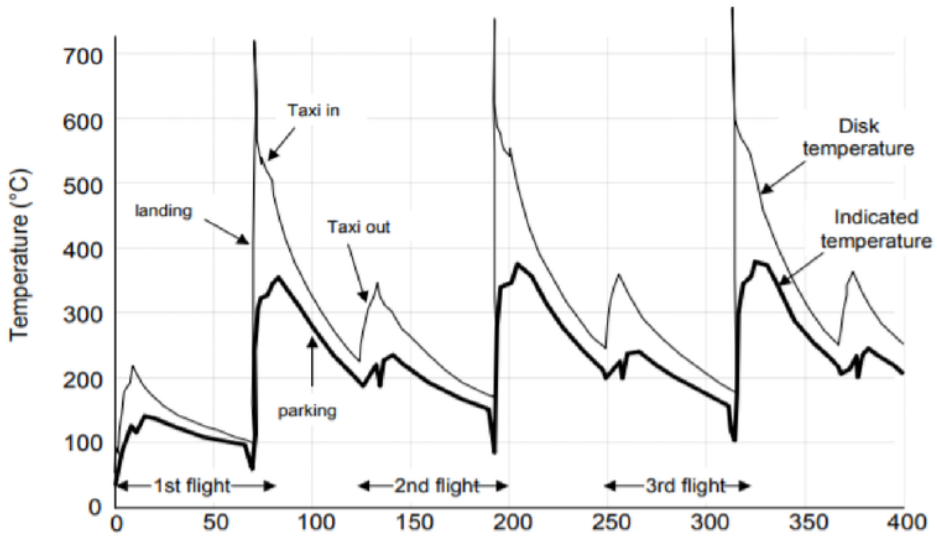


Figure 3 - Carbon Braking System Temperature Management (Airbus, 2014)

3.3 Computational Fluid Dynamics

Any aerodynamic project that utilises computational fluid dynamics (CFD) must endeavour to prove that the settings being used for the CFD provide the most acceptable levels of deviation and error as possible (NASA, 2016). A review of previous studies into the area of CFD, as it relates to ground vehicles, will reveal the best base settings to be used at the start of a user conducted validation study.

This section will detail the various aspects that will be studied during the validation study case for this project.

3.3.1 Reference Geometry

A commonly used validation case study for ground vehicle aerodynamics is the Ahmed body geometry. The Ahmed body is essentially a bluff body geometry, with varying rear slant angles, that gives a representation of the flow seen around automotive geometries (Tunay, et al., 2014) and allows for calibration of CFD settings based on the known, correlated results from previous CFD and wind tunnel experimentation.

The dimensions for the Ahmed body are fixed and shown below in Figure 4.

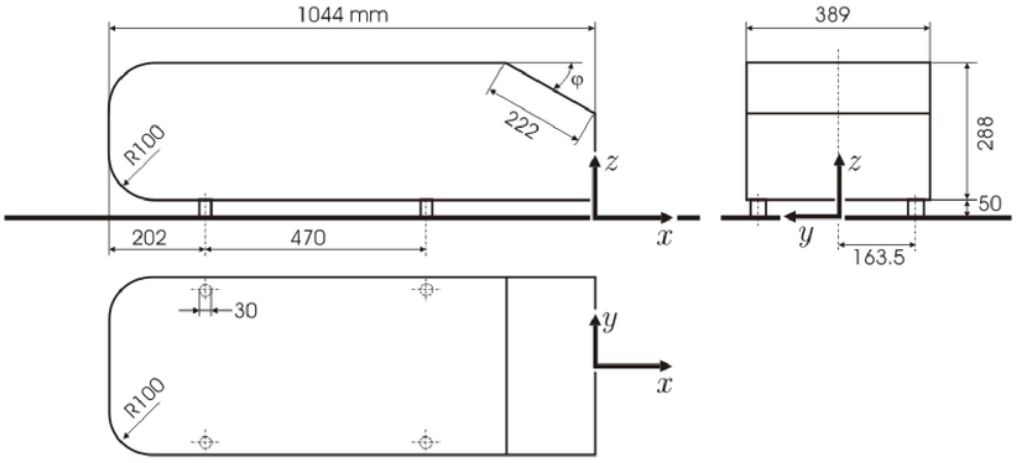


Figure 4 - Ahmed Body Dimensions (CFD Online, 2014)

3.3.2 Domain Sizing

In the context of CFD, the domain size is essentially the 'virtual wind tunnel' that the software will use as the boundaries for the computational solving.

In wind tunnel testing, the dimensions of the measurement cell of the tunnel can have a significant influence on the accuracy of the results obtained due to things like the blockage effect and shear effect from wall interaction (Bernstein & Joppa, 1976). The same issues can be seen in CFD if the domain dimensions are not carefully chosen, as such it is essential to conduct a study into this area.

Many studies have been conducted previously where the authors detail their optimum domain sizes, as per (Rezaeiha, et al., 2018) (Lanfrit, 2005) etc. however it should be said that the specific size is often application dependant. As such, researched values can be used as a valid starting point to reduce computational time, but refinement should still be carried out to achieve output results as close to the known values as possible. In this case (Lanfrit, 2005) suggests a domain of 8x3x3 (L,H,W in geometry lengths) with the domain positioned 3 lengths fore and 5 lengths aft relative to the geometry leading edge.

3.3.3 Mesh Size

CFD software uses a 'mesh' to measure and interpret the fluid flow within all areas of the domain. The type and size of the mesh cells impact the fidelity of the results obtained. (Bakker, 2006) explains that the mesh is used as a discretisation method to allow the software to break the solution down into manageable sections that can be solved within the available computational resources. The dimensions of the mesh cells, and resulting nodal measurement points, will therefore influence the software's ability to detect changes in flow structures within the domain.

In the interest of computing time, it is desirable to have a course mesh that comprises of large cells, although this will have a negative effect on the accuracy of the results. Compromise can therefore be made when generating the mesh, where areas outside the main flow disturbances (the extremities of the domain) that require little monitoring, can be meshed using large elements, while denser areas of mesh can be applied to areas of more interest (around the geometry, in the wake region etc) using smaller elements as per (Ahmad, et al., 2010). The base settings for the mesh investigation will be taken from (Lanfrit, 2005).

3.3.4 Mesh Density Zones

As discussed above, areas of more refined mesh discretisation are required to pick up important areas of flow around the geometry. It is therefore intended to use two differing methods of increasing the mesh density in specific areas, those being Inflation Layers and Density Boxes.

Inflation layers are primarily used to capture the effects of the boundary layer build up on the surfaces of the geometry as well as the road surface (Bathe & Zhang, 2009). These layers add additional cells to the regions where boundary layer interaction with the flow is expected, thus capturing the effects with relative precision. Since it requires relatively significant computational power to generate and integrate these layers into the existing mesh, it is

preferable to restrict the numbers of layers to the minimum required to still achieve good results (Meile, et al., 2010). The initial number of layers to be used for the study will be taken from (Lanfrit, 2005).

3.3.5 Turbulence Models

The software's ability to model the turbulent flow that occurs around the geometry is critical to the accuracy of the results it provides. Due to this, the method of mathematically solving the turbulence (turbulence model) will impact both the results, but also the computational time required.

The two groups that these models fall into are Large Eddy Simulation (LES) or Reynolds Averaged Navier-Stokes (RANS) with RANS models being less computationally demanding due to the simplified equations used compared to LES (Som, et al., 2012). A popular model commonly used for external fluid dynamics is that of K-Omega, considered to have high fidelity when predicting areas of turbulence, separation and boundary layer interaction (Klinzing & Sparrow, 2009). As explained by (Klinzing & Sparrow, 2009), the K-Epsilon models, especially the Realizable version are considered to very robust for the purposes of external fluid dynamics, with good ability to predict turbulence and recirculation flow structures. The K-E models are generally considered to be slightly less computationally demanding, as well as providing some of the best all round packages for this type of application. For the purposes of this investigation, several time independent turbulence models will be assessed with a view to finding the one that provides accurate results compared to published works while also maintaining a reasonable computational time for the solution.

3.4 CFD Methodology

As suggested by (Lee, 1999), when using a computational software to complete simulations and analysis, it is important for the operator to have a reasonable understanding of the way in which the software operates and performs its calculations, to better inform how to set up the simulation and correctly select the boundary conditions. As such, this section intends to provide an overview of the basic processes and principals governing the CFD software.

As explained by (Simscale, 2016), ultimately any CFD software operates by solving the Navier-Stokes equations to give approximations of how fluid flow around or through a body will occur, the emphasis being on approximation Regardless of considered accuracy, any CFD solution is still only an approximation of what would occur in a full-scale physical environment.

The Navier-Stokes equations, as per (NASA, 2009), determine how the velocity, temperature, pressure and density of a fluid in motion relate to each other. The equations are fundamentally based on the work of Euler but have been extended to account for the viscosity of the fluid. Figure 5 shows the Naiver-Stokes equations.

$$Continuity: \frac{\partial \rho}{\partial t} + \frac{\partial (\rho u)}{\partial x} + \frac{\partial (\rho v)}{\partial y} + \frac{\partial (\rho w)}{\partial z} = 0$$

$$X\ Momentum: \frac{\partial (\rho u)}{\partial t} + \frac{\partial (\rho u^2)}{\partial x} + \frac{\partial (\rho uv)}{\partial y} + \frac{\partial (\rho uw)}{\partial z} = -\frac{\partial p}{\partial x} + \frac{1}{Re_r}\left(\frac{\partial \tau_{xx}}{\partial x} + \frac{\partial \tau_{xy}}{\partial y} + \frac{\partial \tau_{xz}}{\partial z}\right)$$

$$Y\ Momentum: \frac{\partial (\rho v)}{\partial t} + \frac{\partial (\rho uv)}{\partial x} + \frac{\partial (\rho v^2)}{\partial y} + \frac{\partial (\rho vw)}{\partial z} = -\frac{\partial p}{\partial y} + \frac{1}{Re_r}\left(\frac{\partial \tau_{xy}}{\partial x} + \frac{\partial \tau_{yy}}{\partial y} + \frac{\partial \tau_{yz}}{\partial z}\right)$$

$$Z\ Momentum: \frac{\partial (\rho w)}{\partial t} + \frac{\partial (\rho uw)}{\partial x} + \frac{\partial (\rho vw)}{\partial y} + \frac{\partial (\rho w^2)}{\partial z} = -\frac{\partial p}{\partial z} + \frac{1}{Re_r}\left(\frac{\partial \tau_{xz}}{\partial x} + \frac{\partial \tau_{yz}}{\partial y} + \frac{\partial \tau_{zz}}{\partial z}\right)$$

$$\begin{aligned} Energy: &\frac{\partial (E_T)}{\partial t} + \frac{\partial (uE_T)}{\partial x} + \frac{\partial (vE_T)}{\partial y} + \frac{\partial (wE_T)}{\partial z} \\ &= -\frac{\partial (up)}{\partial x} - \frac{\partial (vp)}{\partial y} - \frac{\partial (wp)}{\partial z} - \frac{1}{Re_r Pr_r}\left(\frac{\partial q_x}{\partial x} + \frac{\partial q_y}{\partial y} + \frac{\partial q_z}{\partial z}\right) \\ &+ \frac{1}{Re_r}\left(\frac{\partial}{\partial x}\left(u\tau_{xx} + v\tau_{xy} + w\tau_{xz}\right) + \frac{\partial}{\partial y}\left(u\tau_x + v\tau_{yy} + w\tau_{yz}\right)\right. \\ &\left. + \frac{\partial}{\partial z}\left(u\tau_{xz} + v\tau_{yz} + w\tau_{zz}\right)\right) \end{aligned}$$

$$Coordinates: (x, y, z)$$

$$Velocity\ Components: (u, v, w)$$

$$Pressure: p\ \ Density: \rho\ \ Stress: \tau\ \ Reynolds\ Number: Re\ \ Time: t\ \ Energy\ Total: E_T$$

Figure 5 - Navier-Stokes Equations (NASA, 2009)

As shown in figure 5, the equations are treated as coupled partial differential equations, which must be solved simultaneously to come to a solution. Due to the strong complexity of this computation, the use of computers is now the standard method of solving the equations, hence the rise of CFD software to determine fluid flow, especially when considering that these equations must be solved repeatedly with each iteration of fluid motion, as described by (Rapp, 2017).

As already identified, the CFD process is one that results in an approximate result, not necessarily an absolute result as it would appear in the real world. This is due to several reasons, primarily being the limitations of the software, although the robustness of the

mathematical equations when in conditions that involve high deviation from the previous solution can be questionable.

Any CFD software is reliant on the values that are input by the user, which influence the methods that the solver utilises to compute the equations. Additionally, there is considerable emphasis on the quality of the mesh that is applied to represent the geometry and domain, to discretise the problem. These issues will be addressed during the validation study to ascertain the most accurate method of using the software to match published results for a known case.

When considering the process, independent of the software, it is important to consider that there should be a constant feedback loop between the geometry, simulation and analysis phases of the study. It is expected that the workflow will move through a constant cycle from geometry creation, meshing, boundary conditions entry, solver, post-processing and based on the results analysis a return to the start of the cycle. Figure 6, taken from works by (Alahmer & Al-Dabbas, 2014) shows the anticipated workflow cycle for the CFD process, albeit in a slightly different context.

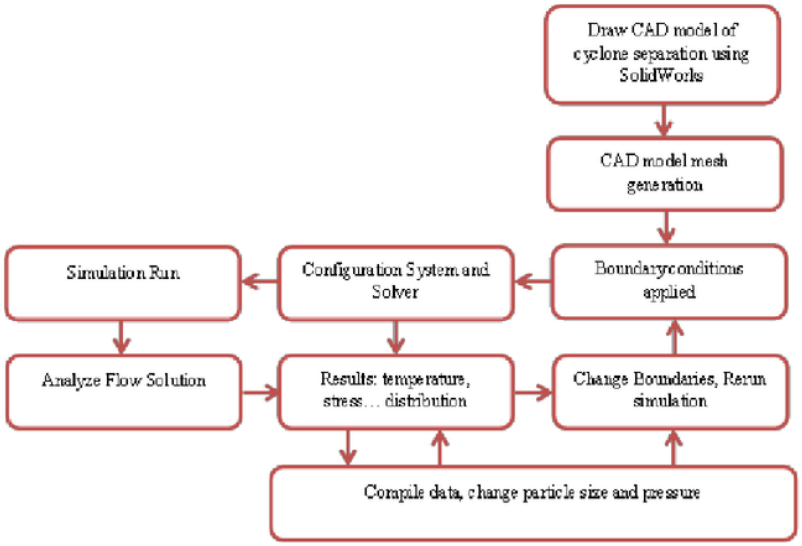


Figure 6 - CFD Workflow (Alahmer & Al-Dabbas, 2014)

3.5 Design of Experiment

It is the intent of this project to conduct a validation study investigation using Design of Experiment (DoE). DoE is a method of designing experiments that can investigate multiple parameters at the same time, allowing for the interactions between the variables to be mapped and analysed, thus providing a deeper understanding of the interactions, as

opposed to taking an iterative approach to parameter sweep testing, as supported by (Collins, et al., 2009).

By using 3 factor, Box Benkham design experiments, it will be possible to sweep through three separate parameters within 17 runs, allowing the software to map the interactions of the variables, thus utilising far less computational resource (Govender & Barton, 2009). Once the experiment is completed, the results input, the software will use a mathematical curve fitting process to analyse the results and provide predictive interactions between the variables, as explained by (Wiley, 2009).

3.6 Turbulent Flow & Wake Structures

Given the focus of study lies on the propagation and management of wheel wake structures, it is important to describe the aerodynamic principles that are responsible for generating this type of wake.

(Houghton & Carpenter, 2003) gives a good description of wake left behind a body moving through air, in that it is rarely seen unless the ambient conditions are right, but the effects on objects nearby or following can often be felt significantly. This is very much the case when looking at wheel wake of open wheel race vehicles, the effects of the wheel wake are seldom visualised, unless in rain conditions, while the influence on the vehicle's aerodynamics, and the resultant impact on following vehicles can be severe.

Another reason why the wake structures are so critical to vehicle performance can be highlighted by the study conducted by (Ahmad, et al., 1984) where it is found that the majority of a vehicles drag is generated by the wake structure formed at the rear of the body. This clearly is not entirely the case in this application, given that the study by (Ahmad, et al., 1984) is based on bluff vehicle body types, while (Wright, 2001) describes the primary sources of drag from open wheel single seaters as being from the wheels and wings. In context, it can be said that the wheel performs aerodynamically somewhere between a bluff body and a cylindrical item when placed in freestream flow, with additional complications incurred from the rotation of the wheels surface making boundary layer determination and interaction very difficult to predict, as found by (Issakhanian, et al., 2010) and supported by (Diasinos, et al., 2015). Figure 7 shows a basic demonstration of the wake formation behind a cylindrical object.

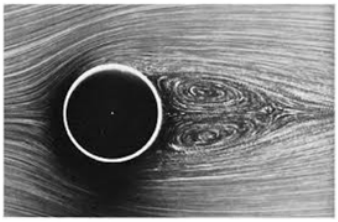


Figure 7 - Wake Formation Behind Cylindrical Object (Wenjun, et al., 2018)

The wake that can be seen in figure 7 is a result of the flow conditions at the front of the body. As explained by (Barnard, 2001), the air that encounters the front of the body generates a stagnation region, where the boundary layer consisting of air that is either stationary or very slow moving relative to the surface it is adjacent to, has enlarged and then captures more of the onset flow, creating a large high pressure zone ahead of the body. This in turn forces more of the onset flow to be directed around the sides of the body, which due to the blockage effect of the body, must then increase in velocity, which can be fundamentally referred to the conservation equations by Navier-Stokes. As a result of the higher velocity flow with associated lower pressure around the sides of the body cannot transition smoothly to the higher pressure zone immediately behind the body, which (Barnard, 2001) explains as being the reason why the lower part of the boundary layer can no longer follow the geometry of the body, and flow separation occurs.

As a result of this separation, there is a loss of momentum in the flow, as shown by (Houghton & Carpenter, 2003), whilst an increase in energy within the flow in the wake region occurs. This energy increase however does not help to smooth the flow back to laminar, but instead creates an eddying effect, resulting in vorticity forming in the flow field behind the body. Much of this research is based on static bodies in a flow field, the whole concept still holds roughly valid for a rotating body like a wheel, with the increased complexity that the boundary layer is constantly acting in a tangential manner to the direction of flow due to the rotation.

These vortices that are generated, (Wright, 2001) describes as being problematic to the downstream components on a race vehicle, given that aerodynamic devices are designed to operate best with a laminar onset flow, whereas the vortices can have a severe detrimental impact. Due to this, it is considered of significant importance by aerodynamicists to find ways of controlling the generated vortices from the front wheels and ensuring they do not impact the performance of downstream aerodynamic devices.

4.0 CFD Validation Study

The following detail the results and understanding obtained from the necessary validations studies conducted in relation to the operation and best practices of the Computational Fluid Dynamics software, Ansys ICEM Mesher and Fluent Solver. Section 3.3 details the parameters that were investigated in these studies.

4.1 Design of Experiment Approach

As detailed previously in section 3.3, DOE software, Design Expert 11, was employed with the intent of being able to use Box-Benkham experiments to map the interactions between the chosen variables. In doing so, this should allow for a broad understanding of the impact changes to the CFD process would have on the results, this being deemed important as the likelihood of having to alter the settings to suit the geometric requirements are high, as mentioned by (Lanfrit, 2005).

2 experiments were designed to map the 5 main variables of interest, domain size, domain position, density box position, mesh element size and number of prism layers. Figure 8 shows an example of one of the experiments.

Std	Run	Factor 1 A:Domain Size Scaling Factor	Factor 2 B:Domain Position Vehicle Lengths	Factor 3 C:Density Box P... Vehicle Lengths	Response 1 Cd %	Response 2 Cl %
4	1	2.5	4.5	0.5	0.45513	0.4186
14	2	1.5	2.5	0.5	0.78164	0.3311
6	3	2.5	2.5	0	1.2002	1.4284
10	4	1.5	4.5	0	0.44055	0.40083
9	5	1.5	0.5	0	0.41606	0.3515
3	6	0.5	4.5	0.5	0.41838	0.35232
17	7	1.5	2.5	0.5	1.2531	1.316
1	8	0.5	0.5	0.5	0.42175	0.37612
5	9	0.5	2.5	0	1.3224	1.2774
13	10	1.5	2.5	0.5	0.4231	0.29464
12	11	1.5	4.5	1	0.42154	0.33881
16	12	1.5	2.5	0.5	0.42153	0.33882
11	13	1.5	0.5	1	0.64181	0.50592
15	14	1.5	2.5	0.5	0.23812	0.20649
2	15	2.5	0.5	0.5	0.45124	0.2982
7	16	0.5	2.5	1	0.64561	0.38471
8	17	2.5	2.5	1	1.1355	1.4163

Figure 8 - Box-Benkham Experimental Design

All CFD runs were conducted in accordance with the parameters laid out by the DOE software. It should be noted that all runs were also conducted using certain standardised settings, detailed in table 1. These settings were kept the same throughout the validation study in the interest of maintaining consistency between runs and ensuring that no undue influence would be imparted on the DOE results.

Setting	Value
Inlet Velocity	40 m/s
Pressure-Velocity Coupling Scheme	Coupled
Pressure Discretisation	Standard
Turbulent Kinetic Energy	Second Order Upwind
Turbulent Dissipation Rate	Second Order Upwind
Flow Courant Number	50
Momentum Relaxation Factor	0.25
Pressure Relaxation Factor	0.25
Turbulent Viscosity	0.98
Maximum Turbulent Viscosity Ratio	10*10^20

Table 1 - CFD Standardised Settings

Table 2 shows the variables tested and the ranges through which they were investigated. Values for the parameters were scaled around a set of base values taken from research of (Ahmad, et al., 2010) (Lanfrit, 2005) and (Azmi, et al., 2017) then scaled accordingly.

Parameter	Range
Domain Size	0.5 – 2.5 Scale
Domain Position	0.5 -4.5 Vehicle Lengths Forward
Density Box Position	0-1 Vehicle Lengths Forward
Mesh Element Size	0.25m-2m
Number of Prism Layers	1-8

Table 2 - DOE Parameters and Ranges

Having conducted both Box-Benkham studies, the results (Cl and Cd figures obtained) were input back to the software and the equation fit process completed.

Unfortunately, due to the significant variance in output values that resulted from the parameter sweeps, and the significant deviation from the target values, the software was not able to fit any equation models with any degree of certainty to the results.

The closest fit to the data yielded only a 23% confidence level from the software, which is far below any acceptable value for any experimental data. It was deemed that the only way to increase the accuracy of the equation fit would be to make the parameter range smaller, although this would result in effectively investigating a small value range from the starting figures, making the validity of the study questionable.

Based on the findings, it can be said that, for broad spectrum CFD studies, with wide value ranges, DOE software is not suitable for task and should not be employed. However, it is still felt that in an optimisation setting, the DOE software would have yielded positive results that would have saved considerable resource.

4.2 Iterative Validation Study

Due to the failure of the DOE approach, a more standardised iterative approach was taken to validating the CFD settings.

As previously detailed, base settings were found based on the works conducted by (Ahmad, et al., 2010) (Azmi, et al., 2017) and (Lanfrit, 2005), with smaller range sweeps conducted either side of these values in an attempt to optimise the values, which are widely accepted. Table 3 shows the starting values, while figure 9 shows the studies conducted and results found.

Parameter	Value
Domain Height	3 Vehicle Lengths
Domain Width	3 Vehicle Lengths
Domain Length	8 Vehicle Lengths
Domain Position Fore	3 Vehicle Lengths
Domain Position Aft	5 Vehicle Lengths
Global Element Size	0.5m
Density Box Element Size	0.025m
Part Element Size	0.01m
Density Box Length	2.5 Vehicle Lengths
Density Box Height	1.5 Vehicle Lengths
Density Box Width	1.5 Vehicle Lengths
Prism Layers	5

Table 3 - Iterative Validation Study Base Settings

Results	Elements	Cl	Cd	% Diff to CFD Cl	% Diff to W/T Cd	Better Than Base	Notes
Base Settings	957932	0.38076337	0.31131417	1.61	-5.53	N/A	Continuity Good, Plots Stabilised
Domain Study							
75% Scale	936409	0.3776618	0.31876136	2.41	-8.05	Worse	Continuity good, stabilised well before itterations ended
90% Scale	971516	0.37618739	0.3156296	2.79	-6.99	Worse	Continuity not as good, Cl never stabilised
110% Scale	1010457	0.38188536	0.31260374	1.32	-5.97	Worse	Cl wavering slightly, but closer, Cd worse
125% Scale	1026919	0.39357025	0.3093172	-1.70	-4.85	Better	Longer compute time, stability reasonable
Mesh Study							
75% Scale	1893496	0.39164016	0.30563186	-1.20	-3.60	Better	Much longer compute time. Stable run.
90% Scale	1255855	0.3628059	0.30880712	6.25	-4.68	Worse	Long run time. Poor results
110% Scale	750955	0.3787646	0.31873771	2.13	-8.05	Worse	Short run time. Not accurate enough
Prism Layers Study							
2 Layers	977912	0.36493876	0.3308505	5.70	-12.15	Worse	Results poor
8 Layers	1026417	0.38503171	0.30798747	0.51	-4.40	Better	Reasonable run time. Suprisingly good results.
Density Box Study							
Vehicle Size Only	248819	0.35760744	0.33843748	7.59	-14.72	Worse	Fast run time. Poor results
50% Larger than Base Size	2938447	0.35416645	0.31257957	8.48	-5.96	Worse	Significantly slower run time
Polyhedra Study							
Base Settings Converted	970092	0.36236291	0.31816479	6.37	-7.85	Worse	Faster run time, poor results
Turbulence Model Study							
K-E Realizable Standard Wall	1026417	0.40089	0.31142	-3.59	-5.57	Worse	No compute time difference, worse results
K-E Realizable Enhanced Wall	1026417	0.39722	0.31759	-2.64	-7.66	Worse	No compute time difference, worse results
K-O SST	1026417	0.32132	0.23011	16.97	22.00	Worse	Poor continuity, bad results, long compute time
Laminar	1026417	-0.063443	0.20009	116.39	32.17	Worse	Terrible
K-E Realizable Scalable Wall	1026417	0.38233	0.3421	1.21	-15.97	Worse	Good compute time, worse results

Figure 9 - Iterative Validation Study Results

Based on analysis of the results in figure 9, it was found that the base settings chosen performed best compared to most iterations, with only 3 iterations yielding results that were closer to the target value for the Ahmed body geometry from (Guilmineau, et al., 2017). Based on the compromise between accuracy and computational time, it was decided that the base settings with 8 prism layers would be proceeded with, given this yielded results very close to the target values while retaining good run times.

While the Cl and Cd figures have been assessed, these can be misleading, and given that the focus of this report is on flow structures, especially turbulent flow, it was necessary to look at the postprocessing images to ensure that correlation can be made between the structures seen from the above selected setting and published material.

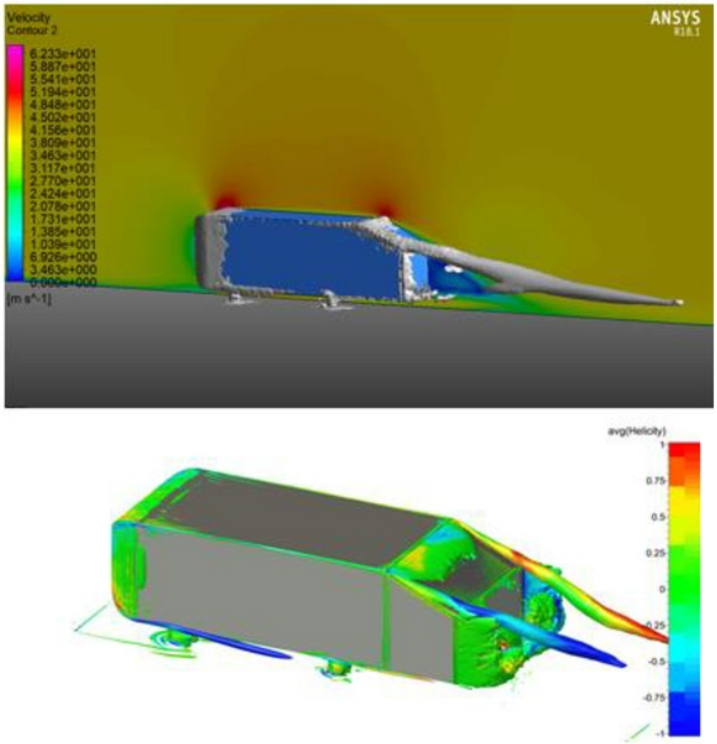


Figure 10 - Ahmed Body Vortex Comparison (Guilmineau, et al., 2017)

Whilst not directly comparable, due to the lower image being taken from (Guilmineau, et al., 2017) and the display settings not being known, there is good correlation between the trends seen in both images. The large trailing vortex that propagates from the slant edge can be seen in both cases, as well as a smaller vortex the begins on the lower corner of the body just after 'nose' section, resulting from the separation effects seen in that area.

The general consistency of results when compared to the published data gives further confidence that the settings being used will yield representative results.

5.0 Brake Duct Investigation

The original focus of study for the project will be around the area immediate to the wheel and suspension, to see if small modifications to the brake duct assembly can be used to sufficiently influence the flow around the assembly.
In conjunction with the aerodynamic studies to be conducted here, another project by Tiegen Lillicrap, looking at the deformation characteristics of composite structures through thermal input, is being referenced with a view to combining the results of both to produce a structure that can be used for aerodynamic gain by altering geometry. Due to this concept, the focus was placed on the brake duct, which is highlighted by an article by (Yares, 2012) as an area of focus in terms of flow management, whilst also having to consider the implications on overall drag and brake cooling issues, as previously discussed in this report.

5.1 Initial Basic Geometry Testing

A series of initial basic geometries were created, with duct geometry based around the concepts currently seen in lower formula cars, such as the Dallara GP2/11 car, an example of which is shown in figure 11.



Figure 11 - Dallara GP2/11 Brake Duct (FIA Formula 2, 2017)

The intent with this section of testing is to ensure the CFD process applied will be suitable to the task, as well as conducting initial computation to strengthen the understanding of the flow structures occurring around the geometry, prior to moving up to larger geometries. Figure 12 shows examples of the geometries created for this phase of testing.

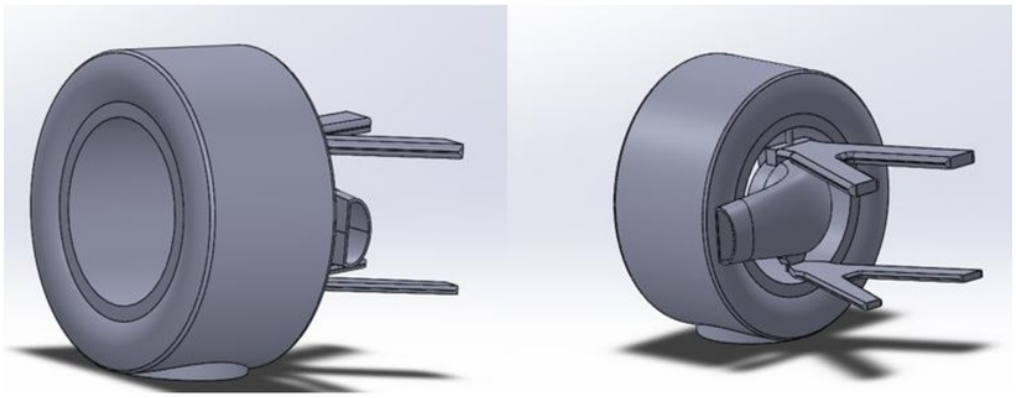


Figure 12 - Simplistic Brake Duct Testing Geometry

An initial CFD run was conducted to examine the basic flow structures seen around the assembly. Figure 13 shows the pressure distribution across the assembly.

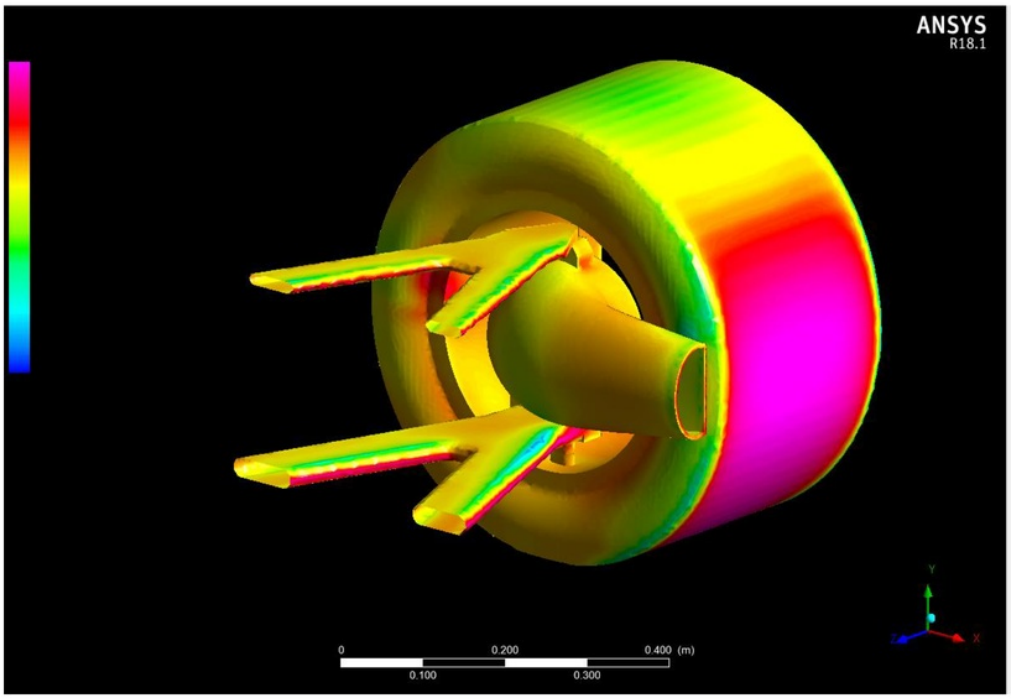


Figure 13 - Brake Duct Initial Run Pressure Distribution

In accordance with what was expected based on the works of (Croner, et al., 2013) and (Diasinos, et al., 2015), a large high pressure zone exists at the fore of the wheel, where the stagnation zone has built as the onset flow encounters the body. Reinforcing the trends that are mentioned in the previously mentioned works, low pressure zones can be seen around the sides of the tyre, and across the top of the tyre, where the flow velocity is increasing as the onset flow must divert around the sides of the stagnation zone, resulting in the lower

pressure areas seen. The pressure differential created around the sides of the tyre can result in undesired side forces being imparted on the assembly if unbalanced side to side, as per (Issakhanian, et al., 2010), although in this case it is found that the differential between inner and outer surfaces is minimal, despite the interaction seen on the inboard surface with the brake duct. It should be noted that most of the difference seen is a result of the throat area that is created between the tyre sidewall and the leading section of the duct, which causes a venturi type effect, resulting in a significant velocity increase, thus lowering the pressure.

When looking at the velocity contours seen at a longitudinal cross section taken through the centre of the tyre, significant differences can be seen to published works.

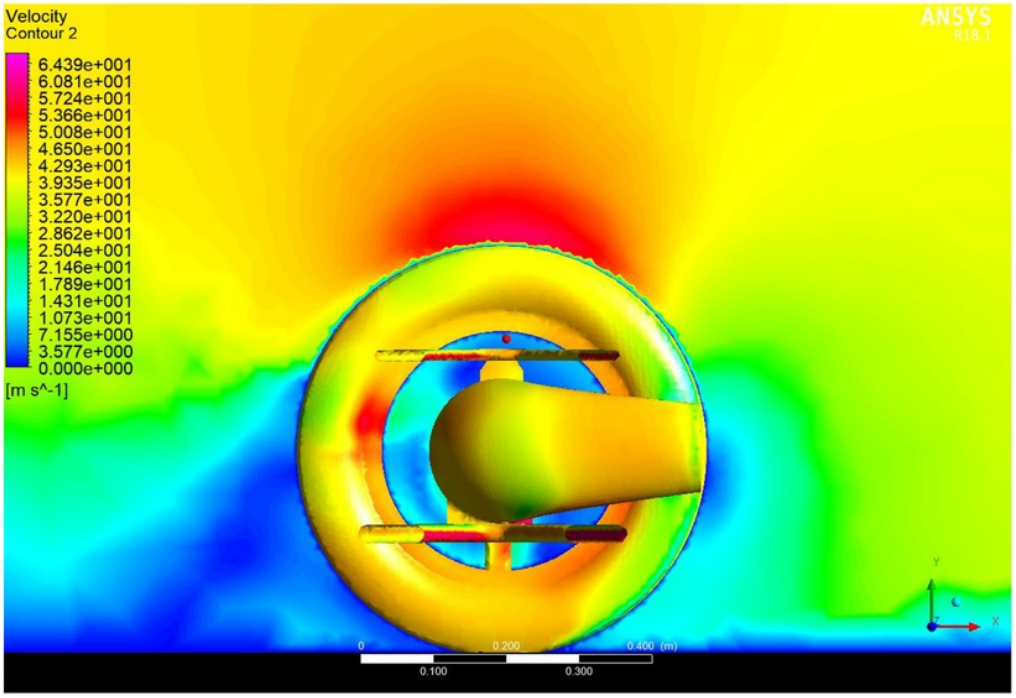


Figure 14 - Brake Duct Initial Run Velocity Contours

The stagnation zone ahead of the wheel can clearly be seen in the area of low velocity flow, which extends down to the road surface, which will be one of the major causes of drag seen on the assembly. The velocity increase over the crown of the tyre is again clear, with the associated reduction in pressure compared to ambient, this will result in much of the lift that the assembly generates, especially given the large surface area it is acting upon in comparison to the other areas of the geometry.

Looking more specifically at the wake structure left behind the wheel, an iso-surface showing the levels of vorticity in the flow field gives a good visual demonstration of the turbulent areas around the geometry. Figure 15 shows the vortex regions.

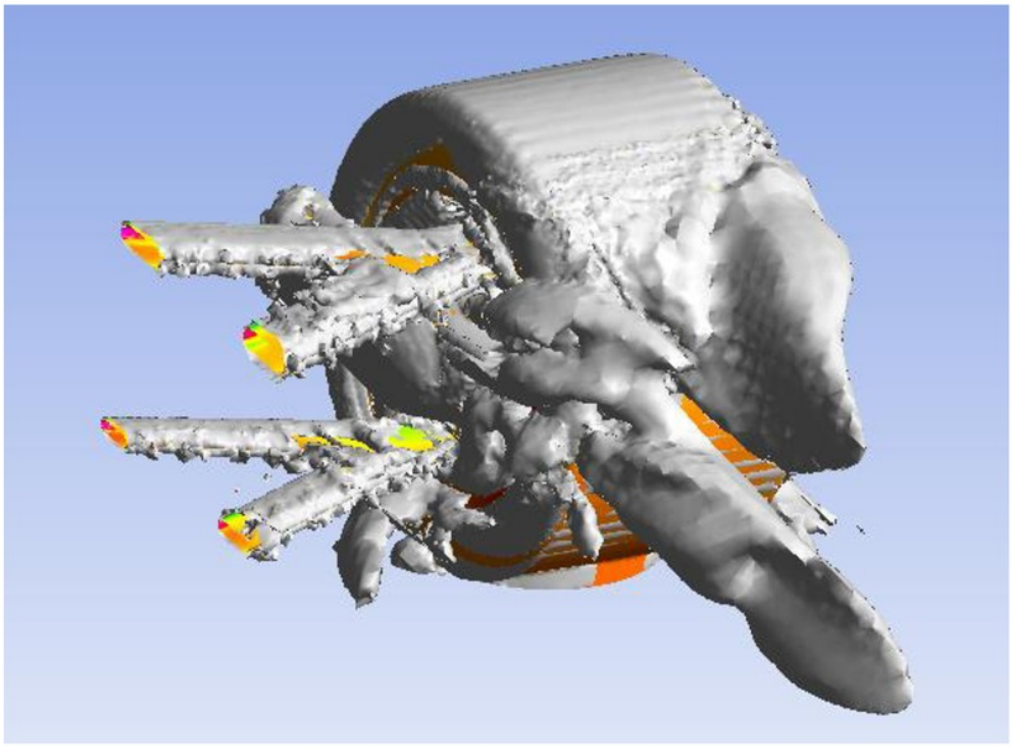


Figure 15 - Vorticity Regions Original Geometry

In keeping with the research detailed in section 3.6, there are 2 large vortices being generated, propagating from the rearward surface of the tyre, where the flow is detaching from the tyre's surface at the rear where there is not enough energy remaining in the boundary layer to maintain attachment of the high velocity flow that has been forced over the top surface.

When looking at a horizontal cut plane through the centre of the axle line, and overlaying the velocity plot, the flow characteristics that are influencing the direction and intensity of the vortices can be seen.

Figure 16 shows two distinct areas of low velocity flow behind the rear of the tyre, the one on the outboard side of the wheel showing significantly lower velocities than the inboard one. On the outboard side, the velocity has dropped to between 0-4 m/s, compared to an onset flow speed of 40 m/s. The resultant lack of energy in this flow will be the reason why the flow separates from the tyre surface on this side significantly earlier, and over a broader area than the inboard side, which follows what would be expected based on the explanations of boundary layer interactions by (Houghton, et al., 2013), resulting in the large turbulent region

seen in this area. Similarly, on the inboard side, another, smaller vortex can be seen, again with an associated area of low velocity flow. Both turbulent regions are bounded by an area of higher velocity flow between then and can be seen to clearly draw towards the centre of the wheel, a result of the pressure differentials being caused by the differing flow velocity regions.

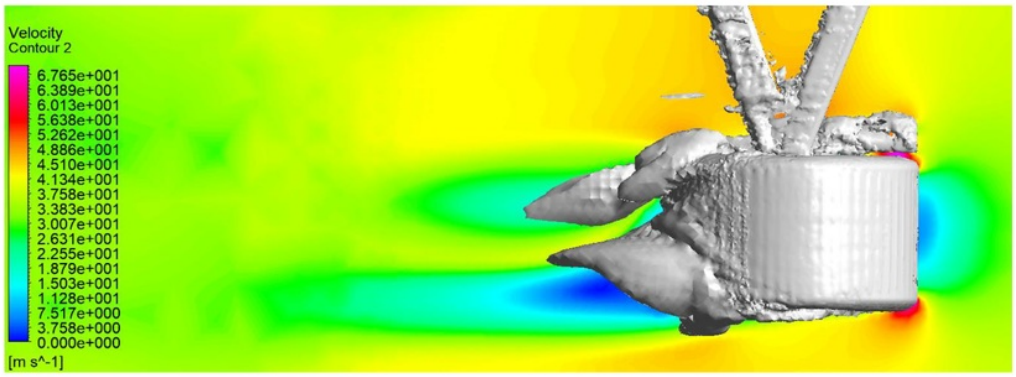


Figure 16 - Brake Duct Initial Run Velocity Profile

The wake formation that can be seen above is in keeping with the trends that were expected, based on the work of (Croner, et al., 2013) (see figure 2) where the formation of vortices behind the wheel occur in very similar manners, even having a larger outboard vortex than inboard. This gives confidence that both the geometry and CFD settings are giving results that are representative of the scenario and can be proceeded with.

5.2 Design Iteration Testing

To determine the feasibility of utilising the duct assembly as a means of flow conditioning, two differing approaches were investigated. Initially a study was conducted into creating slot openings in the duct to reject flow and thereby influence the structures seen around the wishbones. The second study reduces the opening size of the duct, again to reject some of the ingested flow into the duct and redirect it both inside the wheel where it can be absorbed by the flow from the duct, as well as inboard around the duct. Both philosophies will hopefully have a positive effect on the drag implication of the assembly.

5.2.1 Slot Gap Testing

In the interest of reducing the drag implication from the brake duct itself, a series of geometries were drawn up that had slot gap openings, with a surface area of 604.83mm^2. The slot was moved around from the rear section of the duct towards the opening to measure the effects on the flow structures.

Figure 17 shows the first opening position as well as the other tested positions.

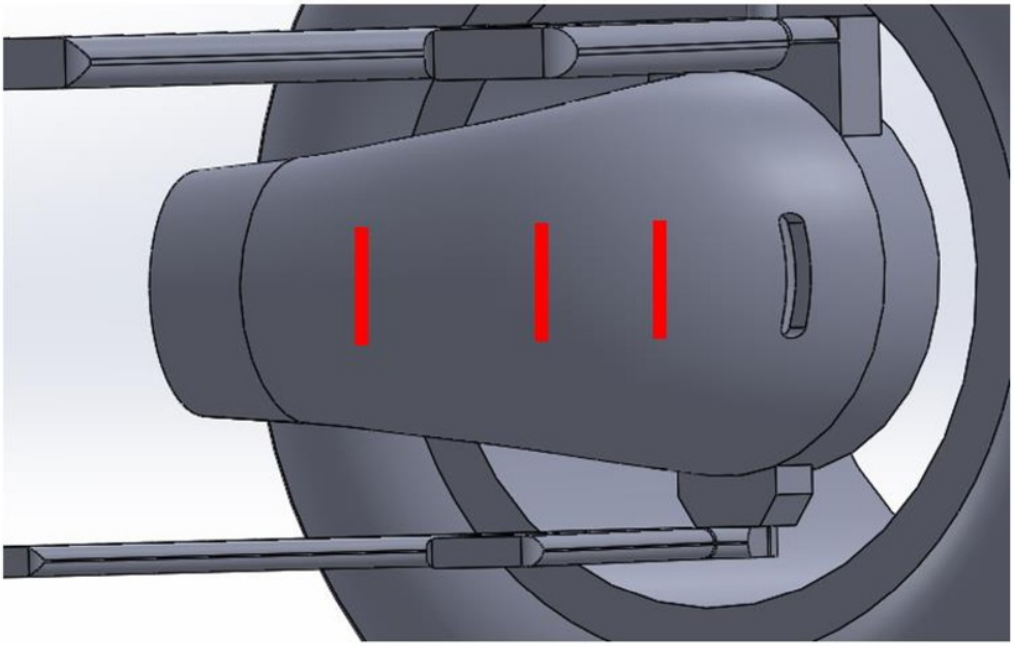


Figure 17 - Slot Gap Testing Positions

Following the CFD runs, the Cl and Cd figures of the components were analysed, results shown in figures 18 and 19.

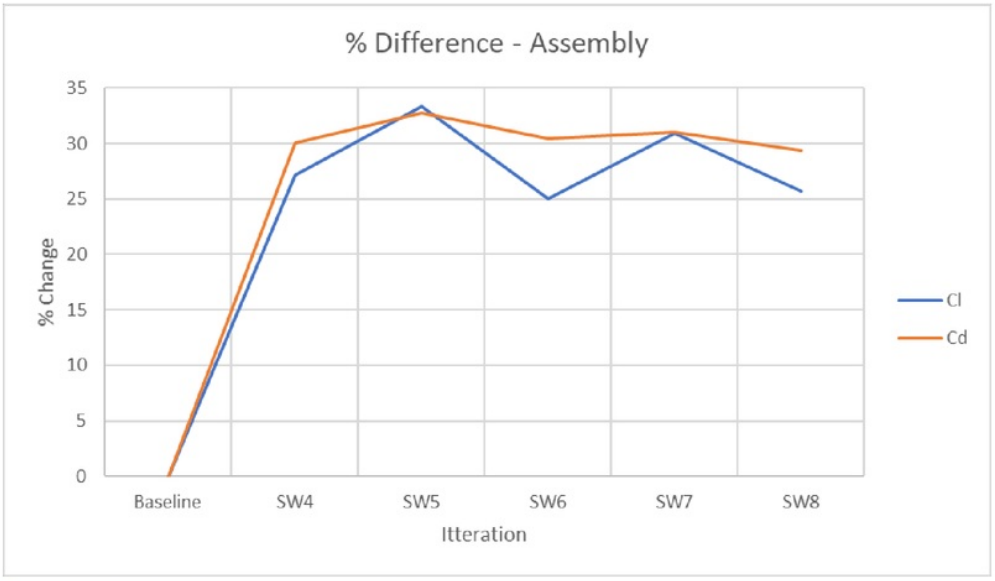


Figure 18 - Slot Gap Testing Assembly Cl Cd Results

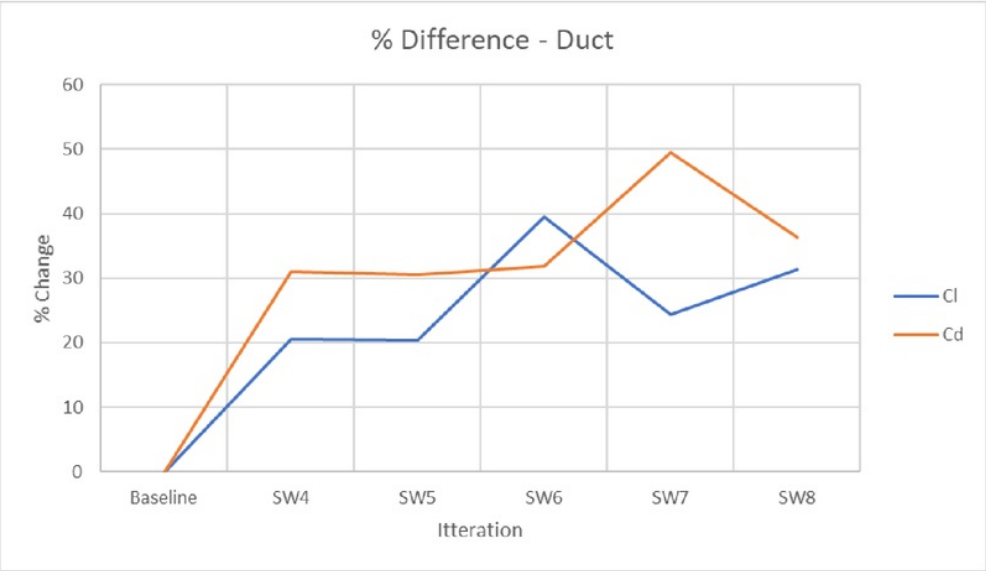


Figure 19 - Slot Gap Testing Duct Cl Cd Results

For all geometries, it was found that all the different configurations of slot positioning had negative influence on the drag and lift values of both the assembly and of the duct when looked at in isolation. This would appear to be a result of the turbulence induced drag that has occurred due to the flow structures seen around the slots, where the rejected flow is interacting with the attached flow around the outer surface of the duct.

Looking at velocity vectors around the slot region, shown in figure 20, there is clearly flow being rejected from the slot, however, because the flow around the exterior of the duct is remaining predominantly attached up to the point of the slot where it begins to separate just prior to the slot, this rejected flow is acting to reenergise this separated flow, resulting in the flow being directed into the edge of the wheel rim. It is unclear what the influence of this would be if the wheel was modelled as a rotating item.

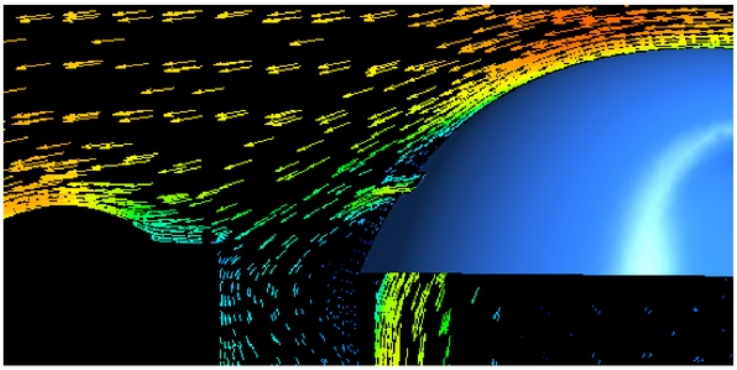


Figure 20 - Slot Gap Testing Flow Vectors

The pressures seen within the duct (figure 21), compared to the baseline have not made any significant change. The region of high pressure at the rear of the duct is still present, the idea of being able to bleed this off with the slot has not happened. It is possible that, with a larger slot, it may be possible to reduce this pressure region, however, the downstream effects of the produced turbulence would likely negate any gains from reducing the internal pressure, based on the vortex regions already being seen from the small slot size.

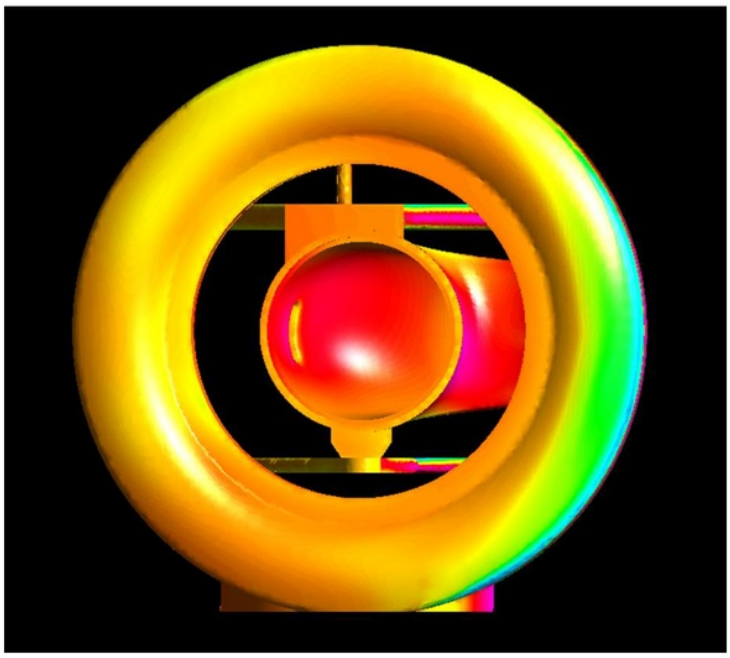


Figure 21 - Slot Gap Testing Duct Pressures

Moving the slot to the forward most position tested has again made a negligible difference to the pressures seen around the geometry. For this iteration, the slot was cut into the duct at an angle of 45 degrees, the intent being to see if some of the high velocity flow entering the duct could be bled off prior to reaching the radius at the rear of the duct. It was also intended to see if redirecting some of this flow between the wishbones would help reenergise some of the disrupted flow seen between the wishbones and smooth the flow downstream.
Looking at the areas of turbulent flow in figure 22, this iteration displays very similar properties to the first slot gap design (as were the other two positions), the only noticeable difference being on the side of the duct around the slot gap itself (below).

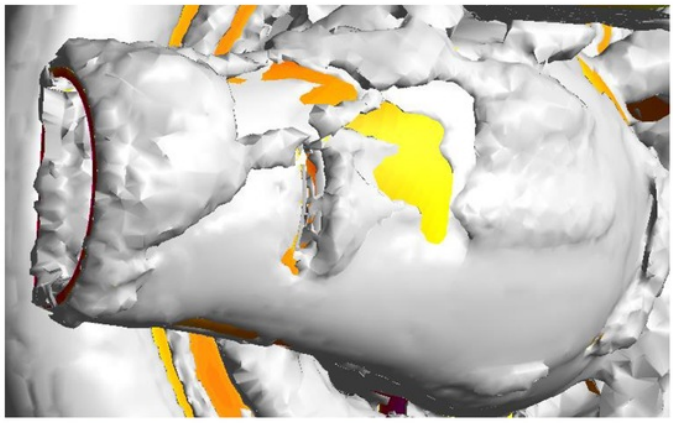


Figure 22 - Slot Gap Testing Turbulent Flow around Duct

As can be seen, the rejected flow is interacting with the attached flow on the exterior surface, causing a region of turbulence around the duct, which is also acting to seal the opening partially, reducing its effective working area. This, coupled with the turbulence seen around the duct opening, will be contributing to making the effective frontal area of the part larger than the base geometry.

When looking at the velocity vectors seen around the assembly (below) with the forward slot gap, there is very little rejected flow seen from the slot into the surrounding airflow structures.

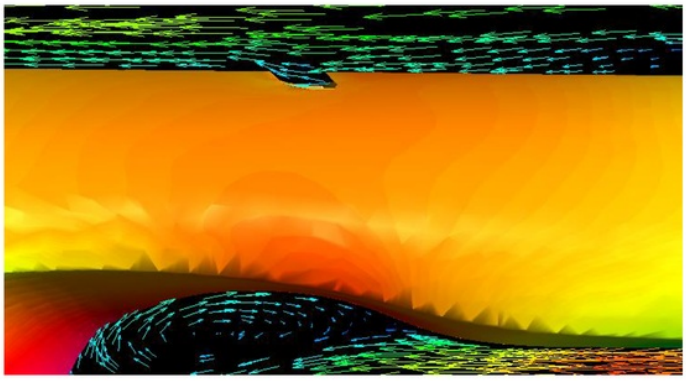


Figure 23 - Slot Gap Testing Flow Vectors Forward Opening

5.2.2 Varied Duct Opening Size

A study was conducted to see the effect of reducing the opening at the duct inlet, to determine the effects on the overall Cl and Cd values, as well as the flow structures seen downstream. The following opening sizes were used:

Opening Size	
Design	Surface Area
	mm^2
Baseline	4611.31
SW9	4335.53
SW10	4064.08
SW11	3801.31
SW12	3545.02

Table 4 - Duct Opening Dimensions

The following results were obtained from changing the opening surface areas.

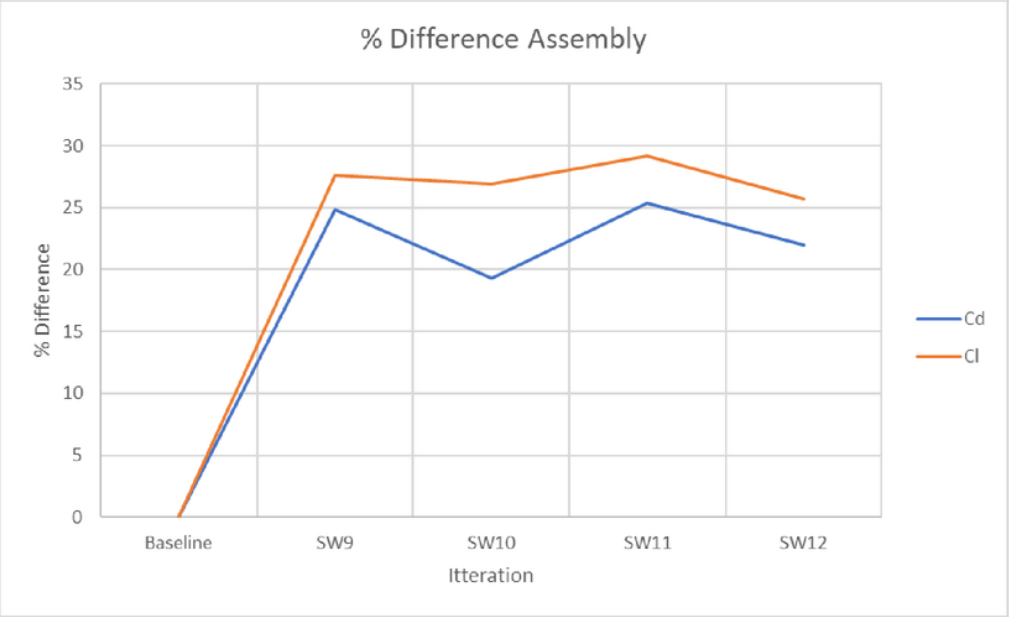


Figure 24 - Duct Opening Size Results on Assembly

As the results show, in all versions, there was a rise in drag and lift values for the assembly and lift. Interestingly, despite the constant reduction in the opening size, the coefficients of lift and drag did not act in a linear increasing or decreasing manner. This implies that potentially the blockage effect that is being caused by the turbulent build around the duct opening

(highlighted in figure 25) is generating more of a sealing effect than closing the aperture itself.

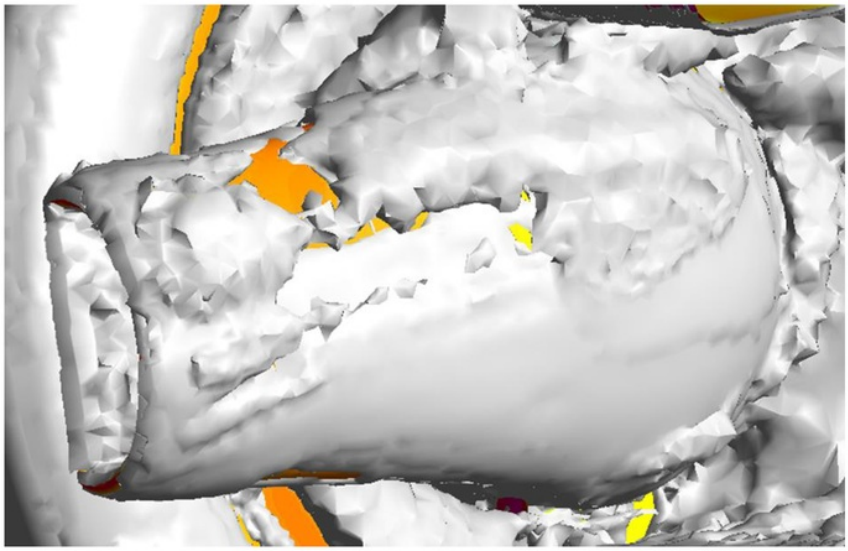


Figure 25 - Areas of Turbulent Flow around Duct

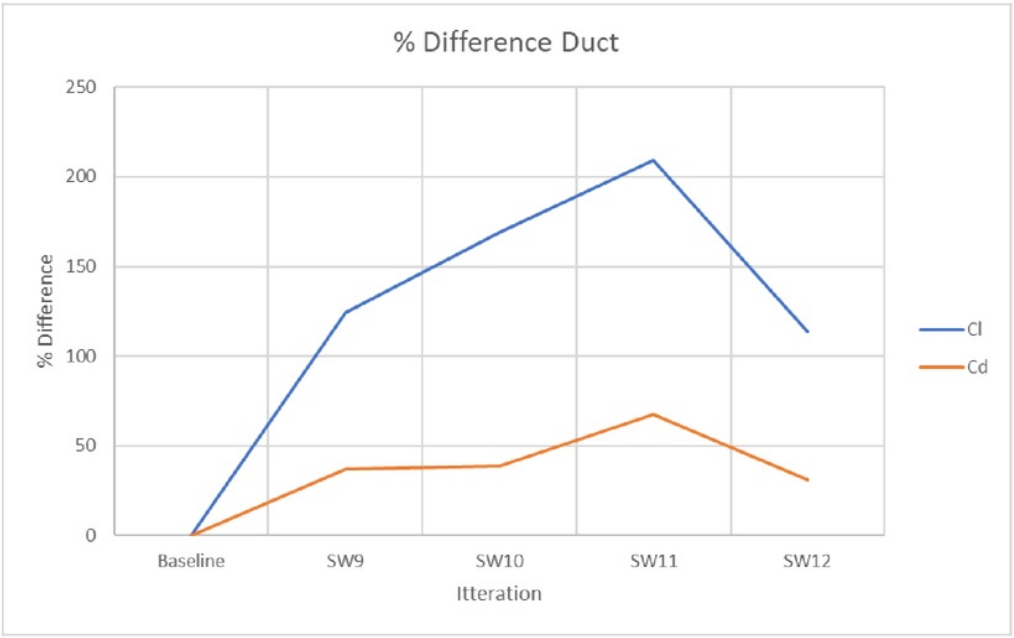


Figure 26 - Duct Opening Size Results on Duct

Looking at the duct in isolation, the increases in values are significantly higher than seen in the whole assembly. Over 200% increase in lift was seen in design SW11, with around 175% seen in design SW10. A rise in values, especially for drag were expected, however this significant change in lift value for the duct was not anticipated. This could be as a result

of the rejected flow being drawn more over the top of the duct as a result of the geometry of the wishbones, given that the duct sitting slightly closer to the upper wishbone, thus increasing the pressure differential seen between the upper and lower surfaces of the duct.

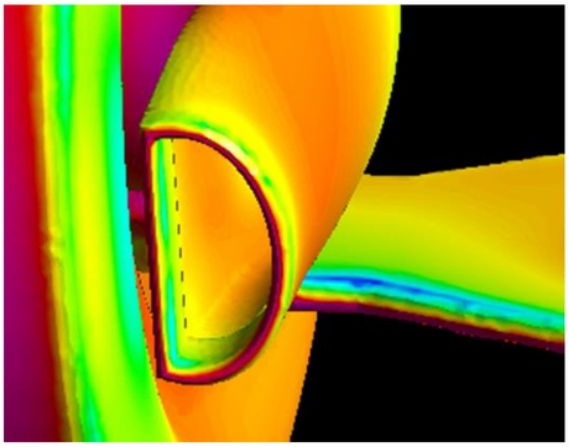


Figure 27 - Brake Duct Opening Tests Pressure Contours

The pressure contours seen in the SW11 version show a significant increase in low pressure seen inside the opening of the duct. It is worth noting that the leading surface of the duct was profiled to reduce the impact of drag on having it as a bluff surface and the reduction in size was not continued all the way through the duct, only the first 50mm. This was done with consideration being given to the idea that a deformable opening would not result in the complete duct tract reducing in size. However, looking at the pressure contours in figure 27, this staggered reduction has resulted in a venturi effect in the front of the duct. There is also low pressure seen around the outer surfaces of the duct opening where the air is now accelerating round the contoured leading edge better than when it was a bluff surface. Although the difference is small, there is also an increase in the low-pressure regions seen around the wishbone regions. It is likely that all of these are contributing to the significantly higher lift values of the assembly seen in these design iterations. Since the trends seen in SW11 will be present in all 4 versions, just to varying degrees with the geometry changes, it is logical that there is a corresponding increase in the lift values seen across the versions.

5.3 Testing Conclusions

After analysis of the results from the testing conducted, there are potential issues to overcome in utilising the brake duct as a means of flow conditioning around the wheel assembly.

The results of the slot gap testing yielded poor results, in that the rejection of flow from any tested point on the duct did not have a significant influence on the flow regimes seen around the component. This is believed to be due to the flow being rejected from the duct being of

lower energy than the flow it encounters, and therefore being predominantly absorbed into the structures it encounters, rather than influencing them, in keeping with characteristics mentioned by (Azmi, et al., 2017). A similar issue has been encountered with the reduced aperture size testing, in that the rejection of flow cannot be easily controlled, and as such is found to have negative impacts on the performance of the overall assembly as it encounters the surrounding flow structures.

Importantly, the testing has highlighted how the flow through the brake duct, which is then rejected through the wheel has an influence on the flow seen moving outboard of the wheel. Figure 28 highlights the direction of the flow through the duct, and how it is interacting with the outboard flow, which appears to maintain the outboard flow in a more parallel direction to the centreline of the vehicle when compared to the inboard flow which draws into the wheel wake more noticeably.

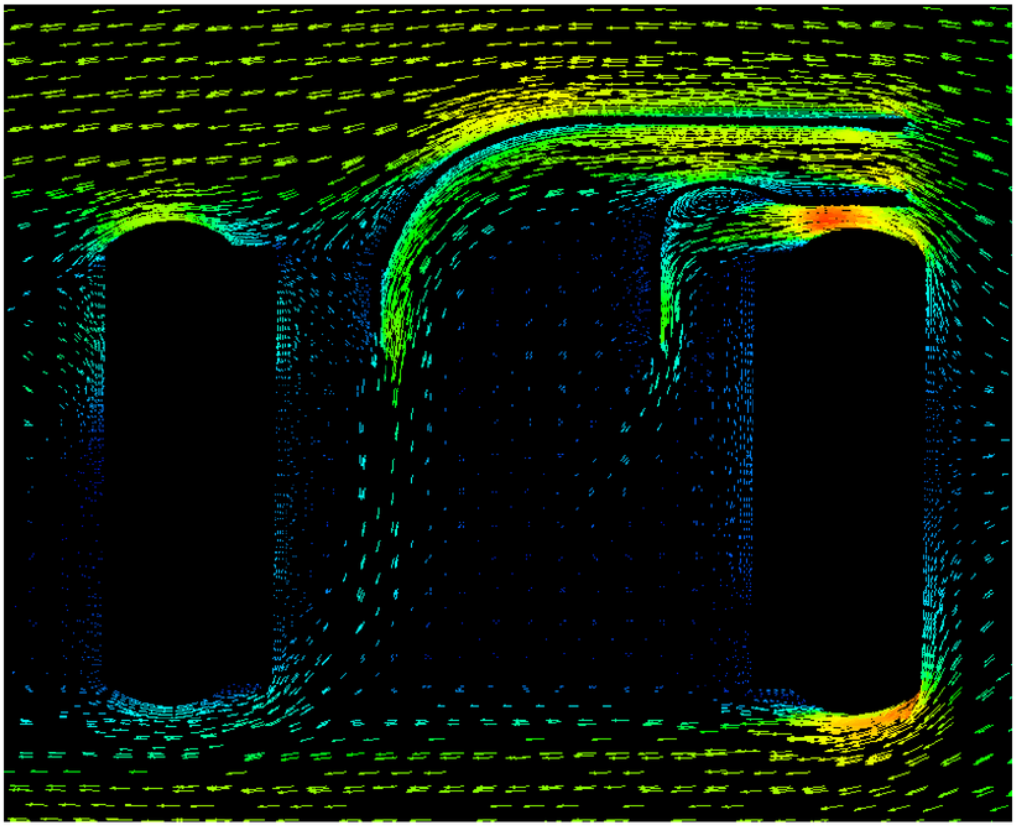


Figure 28 - Flow Vectors showing influence of duct flow

Due to the implied importance on this flow, this testing has highlighted the need, in future testing, to keep the duct as a functioning item to include the influence of this flow in future results.

There are significant errors with this testing, in that the wheel has been modelled as an open item, without spokes or brake components to interrupt the flow, which is highlighted as a significant area of influence by (Motorsport.com, 2016). The decision to not include these influences at this stage was taken to simplify the problem and gain a better understanding of the general flow structures, prior to more refined, representative geometries being tested. Based on this, it can be said that these areas must be included in future geometries to correctly see the influence of the flow through the wheel.

Based on the analysis of results, highlighted in table 5, it can be said that the influence of the duct on the overall corner assembly is very low, thus the ability to influence the overall Cl and Cd values when scaled up to whole car geometries will be extremely difficult to achieve through just the duct geometry.

	Assembly		Duct			
Design	Cl	Cd	Cl	Cl % of Whole	Cd	Cd % of Whole
Baseline	0.558364	0.486152	0.005611	1.0%	0.062259	12.8%
SW9	0.697004	0.62029	0.012599	1.8%	0.085208	13.7%
SW10	0.666313	0.617088	0.015092	2.3%	0.086497	14.0%
SW11	0.700157	0.627998	0.017357	2.5%	0.104351	16.6%
SW12	0.681318	0.611136	0.011988	1.8%	0.081748	13.4%

Table 5 - Cl Cd Results of Duct compared to Assembly

Given the minimal impact of the duct, and the fact that there is significant regulatory change from the FIA constraining the use of brake duct assemblies being use as flow conditioning devices in 2019 and onwards (FIA Formula 1, 2018), it seems prudent to abandon further study into this component, and focus on upstream devices, specifically front wings, and the influence they will have on the wake structures.

It was also clear from the initial analysis of the wake structures seen behind the wheel demonstrate that there is a clear difference in characteristics being caused by the lack of rotation of the tyre surface and the flow remaining attached over the top and down part of the rear surface before separating, contrary to what can be seen in the works of (Croner, et al., 2013) and (Diasinos, et al., 2015). This prompted the decision to run some of the above iterations with the wheel and tyre components modelled in a rotational manner, to achieve better realism. It should be noted that the method used in ANSYS does not rotate the part but applies a tangential vector to any flow contacting the surface based on the velocity of flow and models the boundary layer on the rotating surface slightly differently based on the same method.

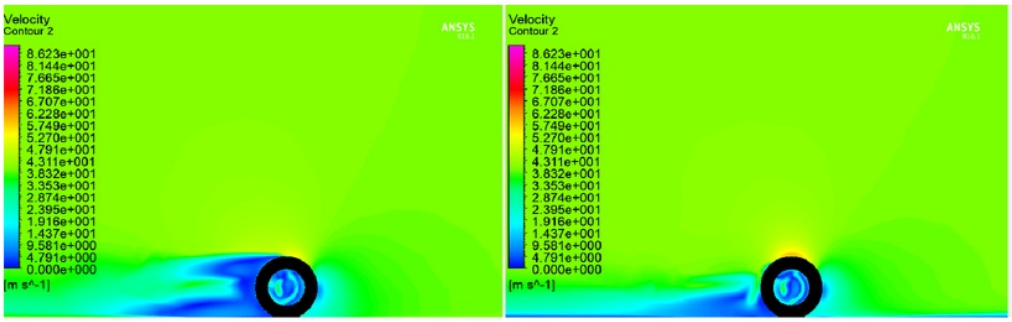


Figure 29 - Rotating Wheel Wake Comparison Velocity Contours

Figure 29 shows the clear difference in wake structures generated, with the rotating version on the left compared to the static wheel on the right. The rotating results now correlate far better to what can be expected, based on (Axereo-Cilies & Iaccarino, 2012), as shown in figure 30.

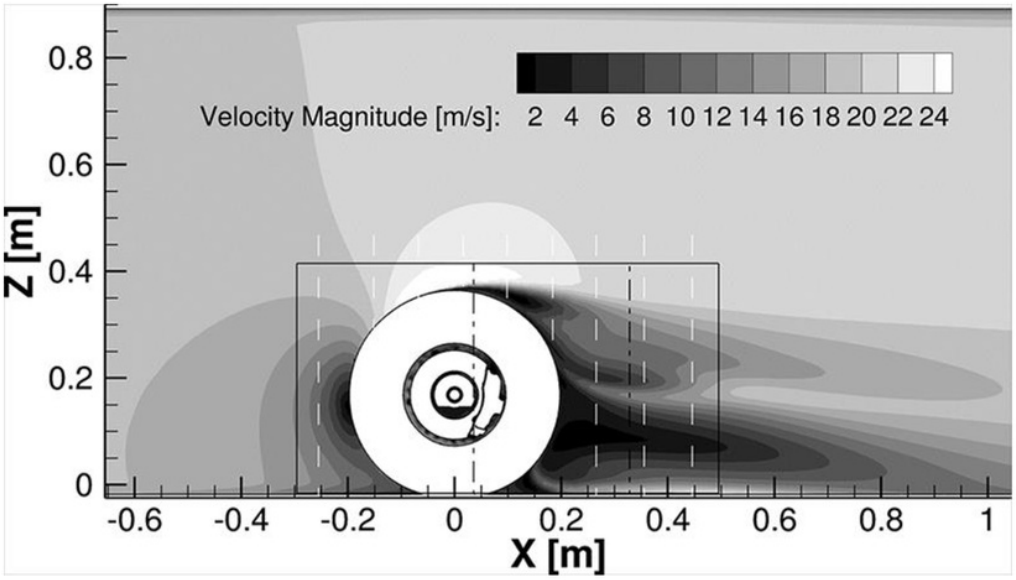


Figure 30 - Rotating F1 Wheel Wake Example (Axereo-Cilies & Iaccarino, 2012)

6.0 Front Wing Design Investigations

An investigation into the potential effects on front wing influence over wheel wake is conducted, informed by the understanding on the general structures and characteristics obtained from the brake duct investigation previously conducted.

Given the recent developments in Formula 1 regarding simplification and regulatory changes governing front wing design, with the intent of restricting team's ability to manage the wake structures seen propagating from the front of the car, as per (FIA Formula 1, 2018), this section of the project will focus on this specific application.

6.1 Representative Geometries

To conduct the study, representative geometries for the front wing assemblies, and complete car models were required. Given that (Wright, 2001) and (Smith, 2013) explain that wing designs in F1 are proprietary, it is impossible to replicate designs that have been used, meaning a representative design is all that can be employed.

The study will utilise 2018 and 2019 wing geometries, along with a representative car model that the wings can be attached to. There are other regulatory changes between 2018 and 2019 in F1 that impact other aerodynamic devices such as the barge boards and rear wings (FIA, 2018). However, to monitor solely the influence of the front wing changes on the flow, it was chosen to neglect these differences and utilise the same car model for all cases tested.

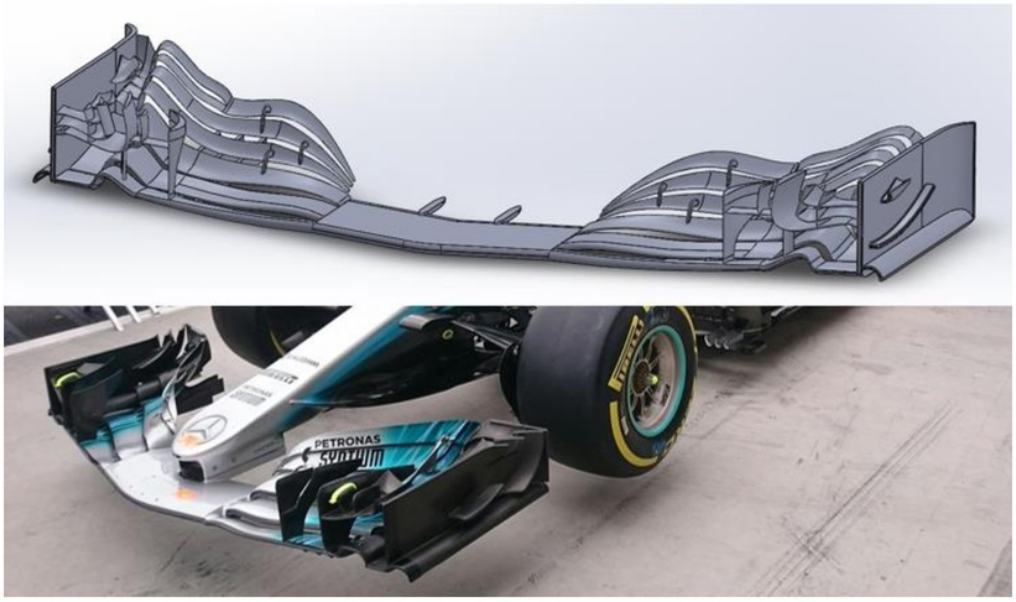


Figure 31 - F1 2018 Wing Geometry (F1Technical.net, 2018)

Figure 31 shows the chosen geometry selected for the 2018 version, credited to (Doodle, 2018). When compared to the image of the Mercedes W08 from 2018, the geometry chosen can be seen to bear close resemblance to the style of wing used.

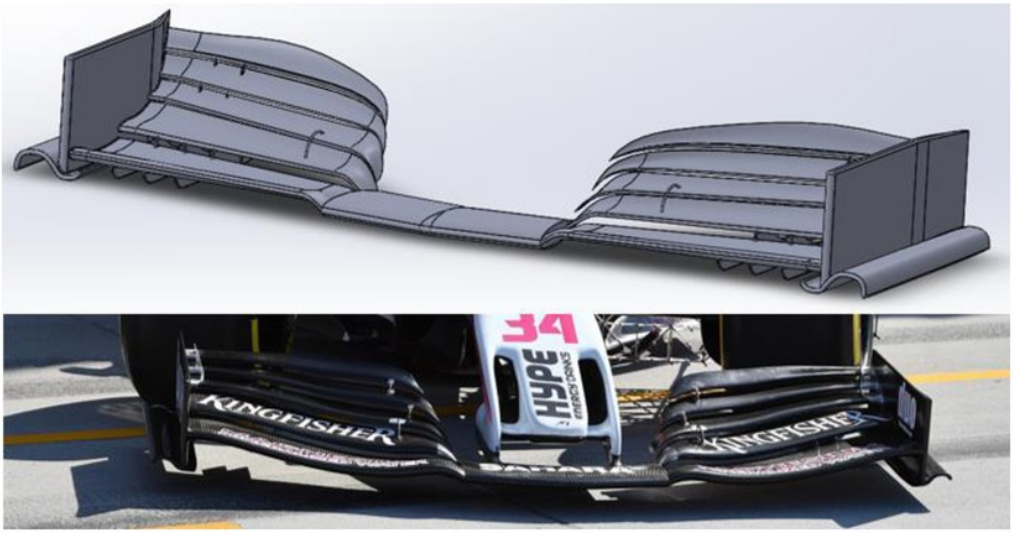


Figure 32 - 2019 Wing Geometry Comparison (FIA Formula 1, 2018)

As figure 32 shows, a similar similarity between a tested 2019 wing design and the selected CAD model, credited to (Petr, 2018).

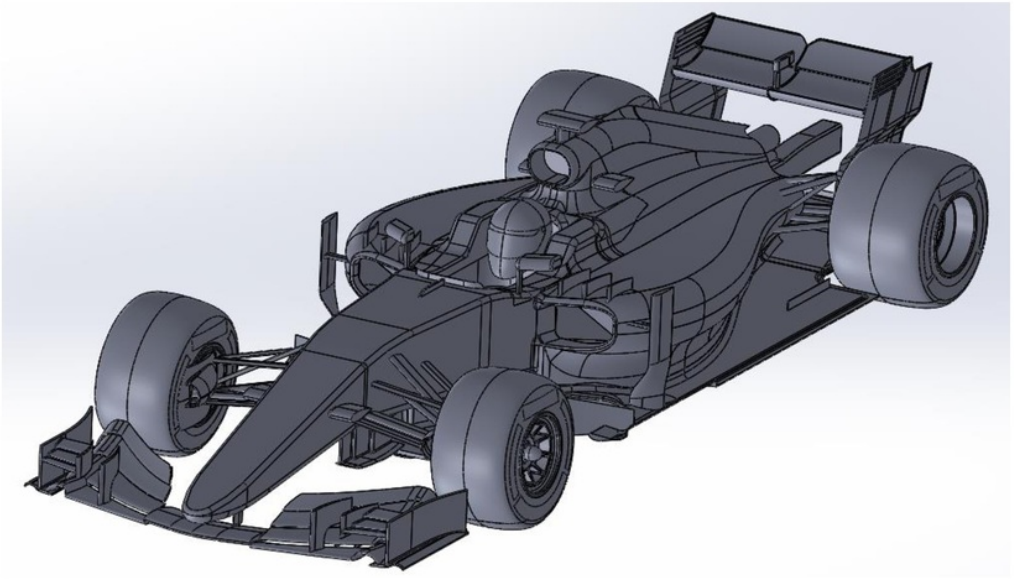


Figure 33 - F1 Car Geometry (Perrinn, 2017)

The chosen vehicle model to attach the wings to was one created by (Perrinn, 2017), which has been utilised in several other studies, and follows the basic dimensions and design

trends seen in F1 cars from the 2018 season. Again, since the design of each car differs and is proprietary, it would be impossible to generate models of each team's cars. By keeping the vehicle geometry standardised throughout the testing, the intent is to see only the influence on flow that the front wing imparts.

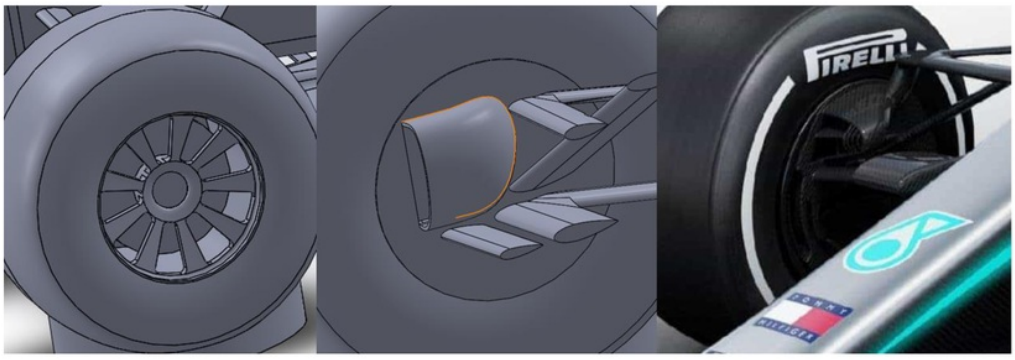


Figure 34 - Representative Wheel and Duct Assembly. Image: (MaxF1.net, 2019)

Based on the findings detailed in section 5, a representative wheel geometry has also been modelled, including a brake disc within the wheel to interrupt flow in a more realistic manner. A working brake duct that is representative of the types found on the 2019 cars is included, along with the inside face of the wheel being blanked, as also seen on 2019 cars as per (MaxF1.net, 2019). Again, these geometries are team specific, as such a generic representative geometry has been created and will be kept the same throughout all testing for continuity.

6.2 Wing in Isolation Testing

To gain an understanding of the general flow structures and differences between the 2018 and 2019 spec wings, CFD runs were conducted using only the wings and nose cone. This was done to allow better visualisation of the flow structures that form from the wing, without the interaction of other components downstream.

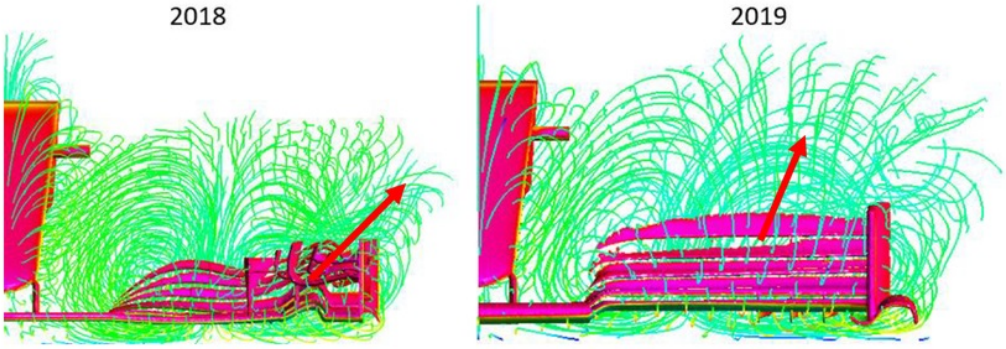


Figure 35 - Wing in Isolation Specification Comparison

Analysis of the streamlines shown in figure 35 initially demonstrate a similar pattern between the two specifications, however on deeper interrogation, there are subtle, yet highly important flow differences visible.

On both wings, there are clearly two vortices being generated in the wake of the wing, one propagating from the inboard winglet tips, and the other being generated on the outboard side from under the main flaps, inside of the end plates. The inboard vortex is known as a Y250 Vortex, based on its position occurring 250mm from the vehicle centreline, where the FIA mandated neutral section and mainplane profile converge. According to (Worldpress.com, 2013), this Y250 vortex forms as a result of the pressure differentials seen between the neutral and mainplane sections, also incorporating the wing tip vortices seen on the end of the flap elements, and is of critical importance to downstream devices such as the leading edge of the floor and barge board sections. A similar vortex can be seen propagating from the 2019 wing in the same location, as would be expected given the neutral section is unchanged, although due to the increased height of the flap element tips, the vortex is noticeably drawing higher with seemingly less control. On this basis, consideration should be given to looking at the position of the flap element tips with a view to controlling the direction of the Y250 in future study.

The primary difference that can be seen between the specifications is in the outboard vortex, which can be seen to be significantly different. On the 2018 spec, the vortex is following an outboard trajectory, being driven by the design of the flap elements and end plate, which it appears are intended to generate an outwash effect. In contrast, the 2019 spec does not have this effect, with the vortex seen to maintain a trajectory parallel to the centreline of the car, negating the previously seen outwash effects. Given that restriction of the outwash is one of the primary intents of the front wing regulation change for 2019, as per (FIA Formula 1, 2018), this can be seen to have been effective based on the initial findings.

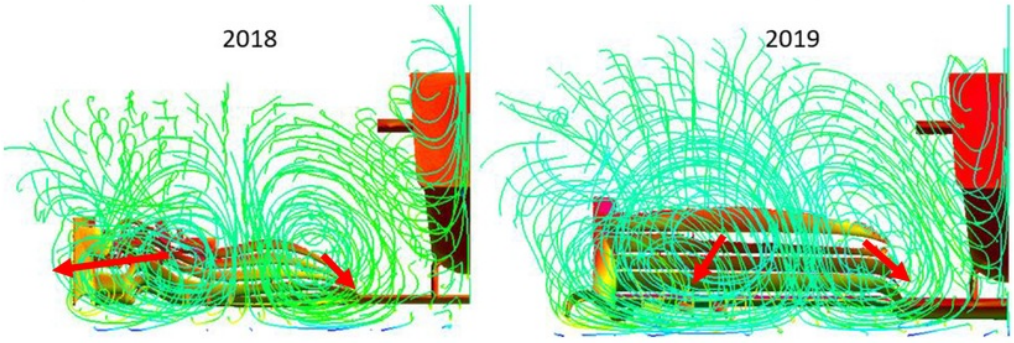


Figure 36 - Wing in Isolation Streamlines Rear View

Figure 36 highlights this difference clearly, showing that the outboard vortex on the 2019 version has a larger propagation, with minimal outwash and can be seen to be interacting

with the Y250 vortex, which is likely to produce undesirable results if found to influence the Y250 trajectory.

Given that the study by (Hetawal, et al., 2014) found significant gain could be obtained in drag reduction by managing flow outboard of the rear wheel, utilising the front wing, it can be assumed that the outwash effects seen would be preferable to the 2019 flow structures. Based on this, differing geometries will be created that attempt to recreate this type of outwash, while staying within the regulatory restrictions imposed, driven by the designs seen during F1 2019 pre-season testing.

6.3 1/3 Car Model Design Testing

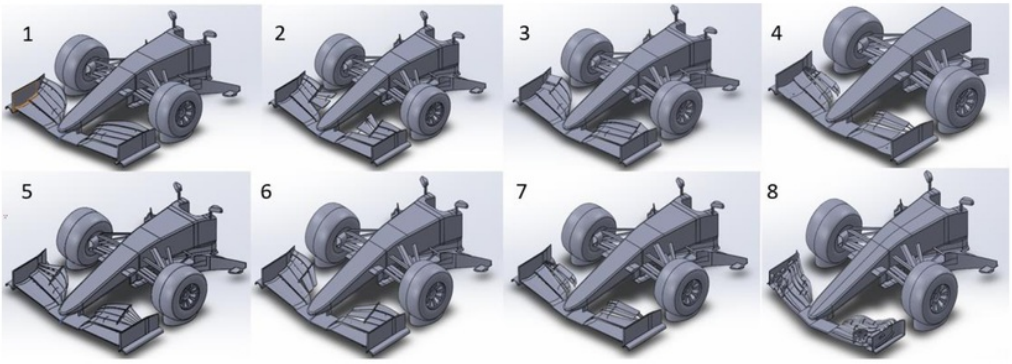


Figure 37 - Design Concepts

With an understanding of the way the front wing is conditioning rearward flow from the isolated testing, the next phase of testing scaled up to 1/3 car models, as shown in figure 37, with varying design concepts created, with differing philosophies to study the impact of flow management. These concepts have been influenced by the designs seen produced by current F1 teams during week 1 of the 2019 pre-season testing. Given that the teams are trialling differing design philosophies, it was decided to test geometries that bear similarity to those seen on circuit, given that it can be assumed the teams will be running concepts relevant to the topic of investigation.

Given the geometry is symmetrical, the decision was taken to split the geometry down the centreline. By modelling the geometry in this way, and using a symmetry-based boundary in ANSYS, it is possible to capture the correct flow characteristics, while reducing computational time.

Table 6 details the designs and the reasoning behind the specifics of each design.

Design Number	Design Name	Design Philosophy
1	2019 Base Spec	Basic specification design following 2019 regulations with no deviation from original FIA intent.
2	Upwash Inner Flaps	Inner flap elements profiled upwards to move Y250 vortex higher and more inboard
3	Outwash Large Flap Elements	Outboard sections of flap elements profiled to direct airflow around tyre, in conjunction with end plate angle, intent to create outwash while maintaining large surface area for maximum downforce production
4	Aggressively Reduced Area Outwash Design with Twisted Mainplane	Significantly reduced upper flaps, with large opening areas outboard to encourage airflow into an outwash condition. Twisted mainplane intended to create a throat effect at outer edge and enhance outwash effects
5	Reduced Area Outer Flap Elements	Reducing frontal area on outer flap sections, and profiling elements to encourage outwash, allowing air a path of least resistance
6	Downwash Inner Flaps	Intended to use wingtip vortices to encourage the Y250 vortex inboard and downwards to interact with floor
7	Aggressively Reduced Area Outwash Flap Elements	As design 4, but keeping the horizontal mainplane for maximum downforce generation
8	2018 Base Spec	For comparison to previous years designs that were heavily profiled to condition flow around front wheel

Table 6 - Design Concept Details

All concepts were tested using identical CFD settings to ensure comparable results. On analysis of the results, there is a significant variance in the Cl, Cd and efficiency values for each design, as highlighted in figure 38. Cl has been plotted as absolute values.

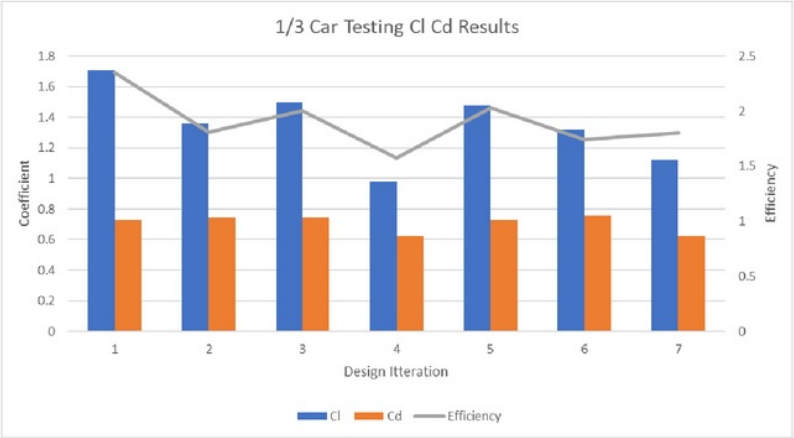


Figure 38 - 1/3 Car Testing Results

The results show a significant increase in the Cl values for all the 2019 style designs over the 2018 base spec. This in part follows the expected trend, in that the larger planar area of the wing, resulting from the width restriction increase, has increased the surface area for the pressure differential to act upon, as would be expected based on (Houghton & Carpenter, 2003). Additionally, the flap elements have also increased in size, again allowing for a greater level of downforce generation.

Due to the increase in area on the wing, it was expected to see an increase in drag as a result, which has occurred in the results, although to a lesser extent than anticipated. It should be noted that the wing accounts for a small amount of the projected frontal area of the model, and when looking at figure 39, an extremely large wake region behind the cut off cockpit section can be seen, forming a recirculation region that will be imparting a large amount of drag on the body, as explained by (Wenjun, et al., 2018).

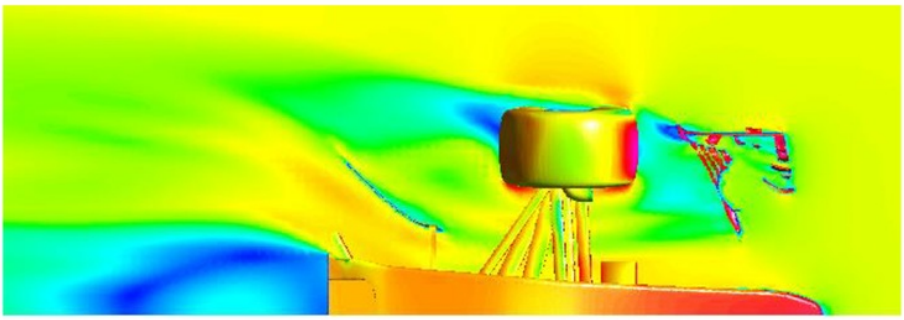


Figure 39 - 2018 Spec Velocity Cut Plane 0.2m from ground

Due to this, the values from these tests cannot be taken as an absolute indicator as to the performance of the designs when scaled to a whole car but give a representative idea of the performance implications and flow structures being generated.

To see how the designs have performed in terms of managing the tyre wake, a cut plane was insert 0.2m above the ground plane, with velocity contours plotted (scaled 0-70 m/s). All designs are shown, numbered to match that shown in table 6.

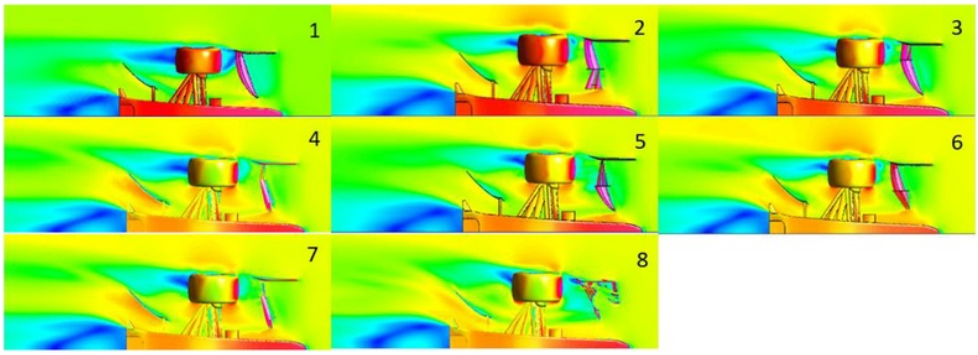


Figure 40 - 1/3 Car Testing Wheel Wake Velocity Cut Planes

The 2018 base (8), shows a considerable outwash effect being generated, drawing the low velocity region in the tyre's wake outboard significantly. This follows what was expected when looking at the wing in isolation, where the larger outboard Von Karman vortex was following at outward trajectory. The influence of this can clearly be seen in figure 40, with the vortex still encountering the tyre face, but due to the trajectory, is drawing around the edge and continuing outboard, thus drawing the wake field with it. Given that (Hetawal, et al., 2014) and (Diasinos & Gatto, 2008) both demonstrated, that by utilising the front wing's wake/vortices to move flow around the front wheel, whilst also keeping this turbulent flow away from the downstream sections of the vehicle, can have beneficial effects in terms of drag reduction as well as ensuring better managed onset flow to downstream devices. On this basis it would appear that the trend seen in the 2018 specification wing would be highly desirable.

The base specification 2019 wing (1) however shows that this outwash effect has effectively been eliminated, with the tyre wake continuing back parallel to the car centre line, again in keeping the vortex propagation seen in the isolated wing study. As already mentioned, this turbulent wake encountering downstream devices is likely undesirable, but does follow what was intended by the FIA regulation change.

Given that it would seem the best option for managing the wake would be to move it outboard of the vehicle, replicating the wake structure seen in the 2018 version would seem the most prudent option to proceed with. Designs 4,5 and 7 all shows very similar wake patterns to that of the 2018 wing, with a clear outwash effect seen in all, design 7 most closely representing that seen in the 2018 design. Figure 38 however shows that these designs have amongst the lowest Cl values of the 2019 designs tested, which was expected

as these designs all have the smallest upper flaps. Figure 41 shows the pressures seen across the undersides of the wings on these designs.

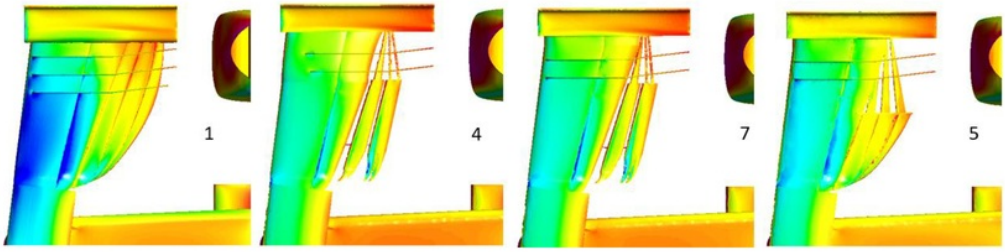


Figure 41 - Pressures on Wing Undersides Designs 1,4,5,7

The base 2019 (1) has a significantly lower pressure across the main plane of the wing when compared to the other designs. The amount of low pressure seen on each design is in keeping with the Cl values seen for these designs. This analysis shows that by changing the geometry of the upper flaps to produce the desired outwash effect, the effectiveness of the flaps to drive the flow under the mainplane, in a compound wing effect as per (Jamei, et al., 2016) whereby the upper flaps help to draw the flow around the main wing and retain attachment further along the surface, has been eroded, reducing the effectiveness of the wing as a whole.

This loss of front end downforce may be problematic, given that both (Wright, 2001) and (Smith, 2013) both describe balancing the vehicles centre of pressure (COP) (the point about which the front and rear downforce moments act upon (Houghton & Carpenter, 2003)) and mass distribution is critical to handling balance. Due to the reduced front wing effectiveness, the COP may have shifted too far rearward for the application. This cannot be investigated until whole car geometries are studied.

Given that the potential COP issue, and the fact that that while the flow structures around the front wheel can be seen, the downstream effects of where these flows end up cannot be seen unless studied on a full car model. On this basis it is necessary to conduct the same studies, on full car geometries.

6.4 Full Car Geometry Testing

Using the previously detailed full car geometry, all front wing designs were attached, with the correct geometric constraints as per their associated regulations (FIA, 2018), and CFD runs conducted using identical boundary conditions and mesh settings. It should be stated that mesh settings were adapted slightly case to case to meet the requirements of the individual geometries. Whilst changes were kept as minor as possible, there may be some slight influence seen on the results, although this is expected to be minimal.

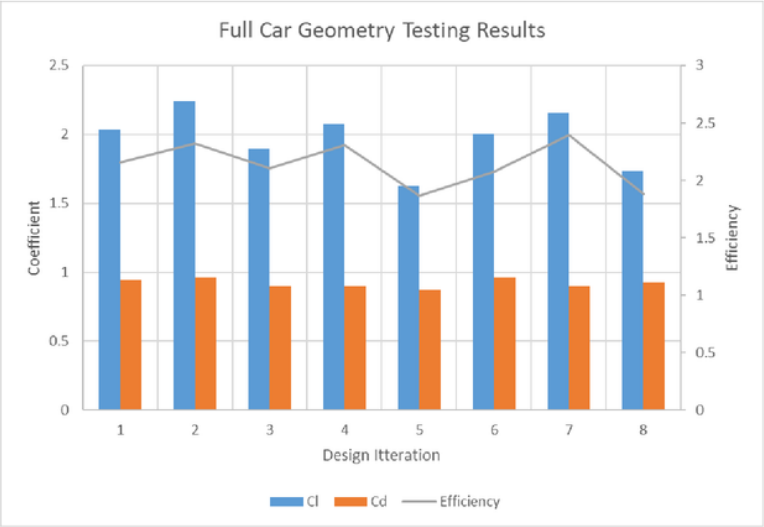


Figure 42 - Full Car Geometry Testing Results

The values obtained from the testing are shown in figure 42. Interestingly, now some of the more promising designs, namely 4 and 7 are showing significantly higher Cl values than when tested as 1/3 car models. This shows that the downstream influence of the flow management at the front end is having a positive impact, validating the decision to attempt to achieve larger amounts of outwash with the designs being seen produced by teams.

In terms of efficiency, designs 4 and 7 are more efficient than the base 2019 spec by 7% and 11% respectively. Given that both (Smith, 1978), (Smith, 2013) and (Houghton & Carpenter, 2003) all make mention of an aerodynamic body's efficiency being just as critical to its performance as its ability to solely produce lift (or downforce in this case), it can be taken that downforce at the expense of excessive drag will not necessarily be beneficial to lap times. Considering designs 4 and 7 have Cl values higher than the 2019 baseline version, and lower drag, while previous analysis has shown the front wings are not working as well, it can be assumed that the flow control by the front wing is having a significantly positive effect on the effectiveness of the downstream devices.

As previously mentioned however, consideration must be given to the distribution of the downforce across the vehicle, and the resulting centre of pressure is potentially more important than the raw downforce numbers produced.

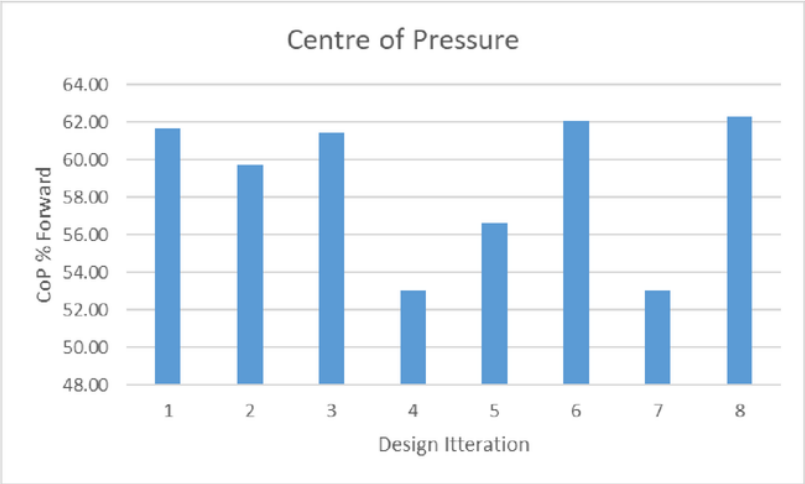


Figure 43 - Full Car Geometry Testing Centre of Pressure Results

Calculating the centre of pressure from the force moments that are found in the CFD results, there is a wide spread seen between the designs. As feared, designs 4 and 7, although having excellent efficiency values, have yielded a CoP significantly more rearward than the other designs. The CoP of these designs can now be found to be only slightly above 50% forward, in contrast to the over 60% of both the 2018 and 2019 baseline designs. Although (Katz, 1995) does state that a neutrally positioned CoP can be beneficial in providing balanced downforce levels on each axle, the exact position of CoP must be paired with the position of the mass distribution of the vehicle. Given that an F1 car is mid-engined, with much of the weight central or rearward, it is likely that the mass distribution is biased to the rear, hence why a more forward CoP would be desirable, to create a more neutral balance. Without further information, and simulator testing, it is impossible to state where the optimum CoP position should be in this context, however the considerable shift in position with designs 4 and 7 does raise concern as to the balance implications, although this could potentially be countered with ballast, as per (Smith, 2013).

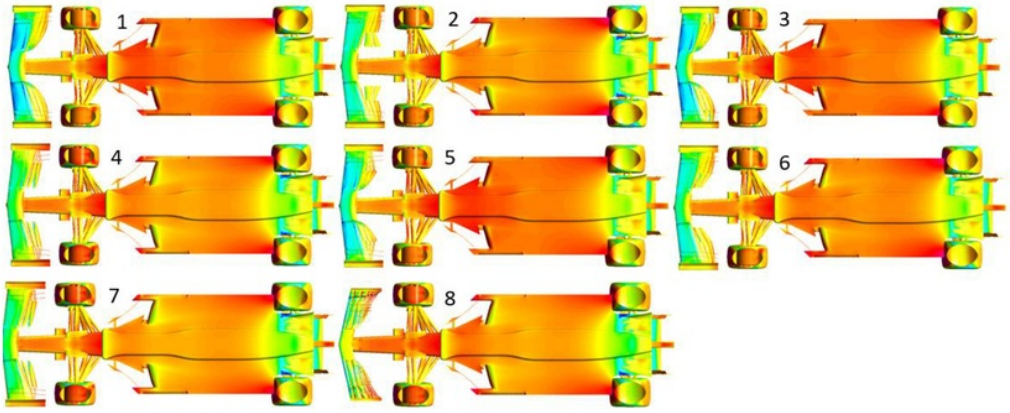


Figure 44 - Full Car Geometry Testing Underside Pressure Distributions

Figure 44 shows the pressures seen on the underside of the geometries, all with the same scaling (-3000 to 1000 Pa) for comparison to determine the areas causing the change in CoP. Designs 4 and 7 can be seen to have noticeably less pronounced low pressure on the front wing compared to the 2019 base spec (1). Contrastingly, the diffuser area on 4 and 7 shows a larger propagation of the lower pressure region ahead of the kick point, along with areas of significantly lower pressure at the edges of the diffuser throat area compared to the 2019 baseline.

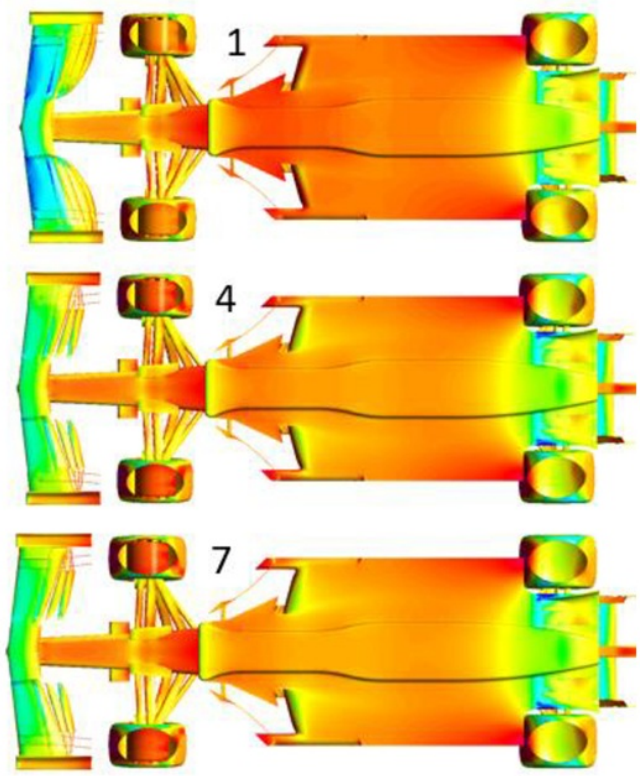


Figure 45 - Full Car Geometry Testing Designs 1,4 & 7 Underside Pressures

Closer inspection shows that the diffuser section on 4 and 7 is working significantly harder than on the baseline, which in turn is driving a pressure drop across the whole floor section when compared to base. This, coupled with the reduction in low pressure under the front wing would account for the shift of CoP value rearward on designs 4 and 7. Interestingly, the leading edges of the floor section on 4 and 7 are experiencing a lower pressure than seen on 1, however any associated increase in downforce in these sections, which are forward of the car centre point, are clearly not enough to outweigh the loss of front wing downforce and gain on diffuser downforce to rebalance the CoP.

From this analysis it can be assumed that the outwash being generated in designs 4 and 7 is having the effect of moving the turbulent flow coming from the front wing and wheel outboard, which is then helping to not disturb the flow under the floor from the sides, thus allowing a smoother and higher velocity flow, resulting in a more effective venturi effect.

Another area to consider is that the differing front wing design is having a significant influence on the airflow to the leading edge of the floor. Figure 46 shows a section view with the velocity contours plotted for designs 1 and 4.

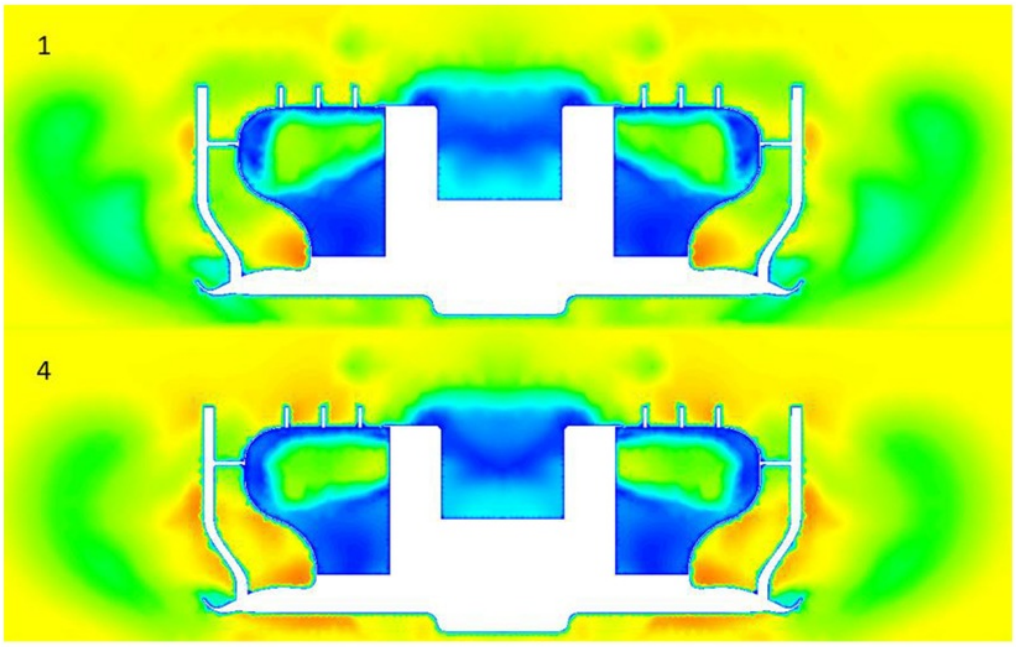


Figure 46 - Full Car Geometry Testing Velocity Cut Plane Designs 1 & 4

Design 4 shows significantly higher velocity flow under the floor sections, in keeping with the pressure plots on the car. Based on statements by (Jamei, et al., 2016) and (Oulton, 1971) it can be said a compound wing structure will generate a greater upwash as the auxiliary elements interact, maintaining flow attachment for longer, thus angling the flow upwards. Given that the base spec 2019 wing (1) has 3 large flap elements that form the compound wing structure, as opposed to the 2 smaller flaps on designs 4 and 7, it is expected that a reduced upwash is generated by designs 4 and 7. This is confirmed when looking at the velocity profiles found on a section view 0.6m from car centre line, shown in figure 47.

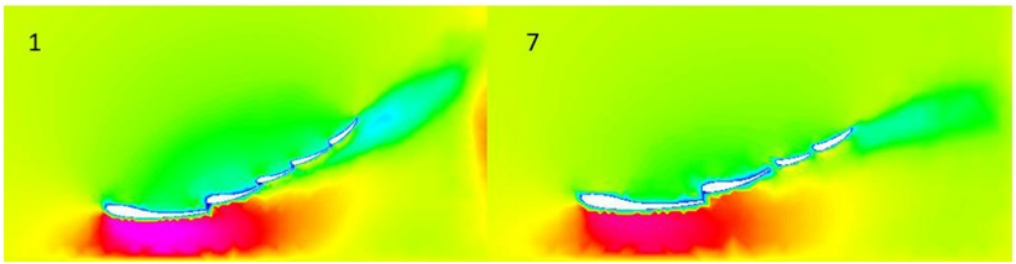


Figure 47 - Front Wing Upwash Characteristics

As verification that the upwash, or lack of, is the primary reason for the increased flow under the floor, figure 46 can be referred to. The high velocity areas of flow on design 4 can be seen lower to the ground plane, with large concentrations below the mid-point of the sidepod, demonstrating how the reduced upwash is allowing more flow under the car. In

contrast, the distribution of flow on the baseline 2019 car can be seen to be far more even across the height of the vehicle. The upwash from the larger wing can also be seen when looking at the flow through the sidepods, where on design 1 the sidepods can be seen to be ingesting a larger amount of higher velocity airflow than in design 4.

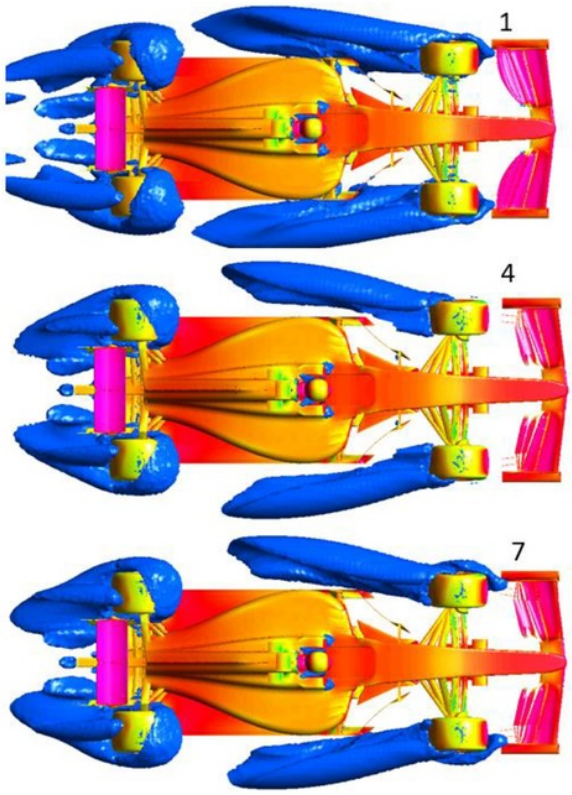


Figure 48 - Full Car Geometry Testing Turbulent Kinetic Energy Isosurface

An Isosurface is imposed showing the regions of turbulent kinetic energy (at 42 m^2 s^-2) to ascertain the effects of the wing designs on the wheel wake. The baseline 2019 wing, with its lack of outwash, results in a large turbulent flow in the wake of the front tyre, where the airflow is directly impacting the tyre face and leaving a large wake once separation has occurred. This contrasts with the two best performing designs, where the turbulent wake left by the front wheel is noticeably reduced.

The intensity of the wake region is of significant note, however more important is the position and trajectory of the wake. In the baseline geometry, the wheel wake can be seen to remain noticeably closer to the side of the vehicle, where it contacts the edge of the sidepod. With both designs 4 and 7, the wake moves considerably further outboard of the sidepods.

The impact of the wake's trajectory can be seen on the regions of turbulence around the rear wheels. Where the wake is not being managed in an outboard manner, a larger turbulent region is present ahead of the rear wheel, whereas this reduces when the outwash effect is stronger.

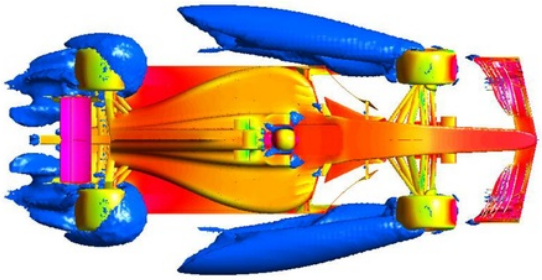


Figure 49 - Full Car Geometry Testing 2018 Spec Turbulent Kinetic Energy

When comparing the turbulent regions found with the 2018 geometry, a very clear similarity can be seen with designs 4 and 7, both in terms of intensity and trajectory of the turbulent flow. Given that the above designs are based around concepts which have been trialled in F1 pre-season testing, it is apparent that the teams are attempting to move back towards flow structures that more closely resemble those from the previous year's regulations. Given that the intent of the regulation change by the FIA was an attempt to reduce the wake of a vehicle to allow another to follow more closely, to give additional context to the investigation it was decided to conduct a limited study with a car following another, to be detailed in the next section.

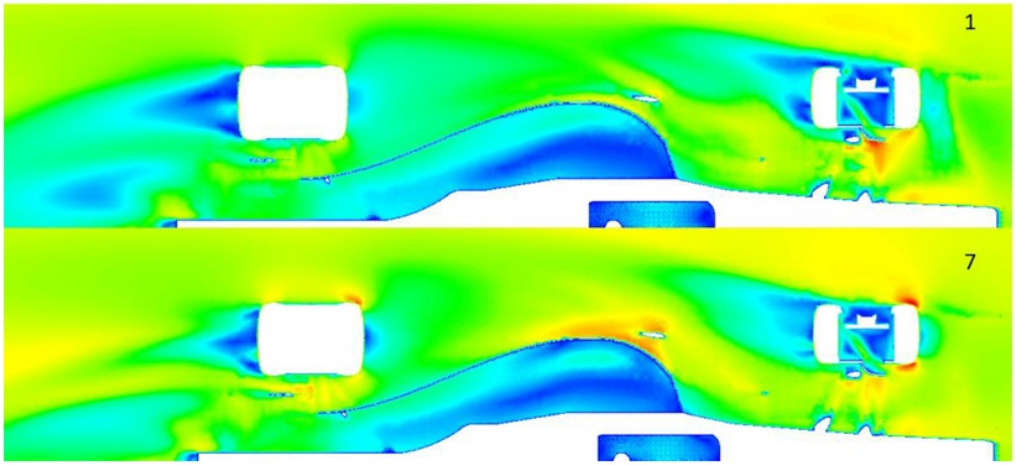


Figure 50 - Velocity Contours Section View 0.35m above Ground Plane

Figure 50, showing a section view at wheel centre line height, give a good visualisation of the differences in flow velocity around the front wheel created by the differing wing

geometries. The reduced flap area of design 7, and the flow conditioning created by the design is resulting in an increased velocity in flow around the wheel, where the flow is being better directed outboard and inboard of the tyre. This is especially prominent on the outboard side of the wheel, which is then causing a far greater outwash effect and drawing the wheel wake outboard from the vehicle.

Figure 50 demonstrates that the design of the front wheel, with the functional brake duct, is having the desired effect of bleeding off flow from within the suspension region, and rejecting it out of the wheel, to then interact with the flow on the outboard side of the wheel. There are still issues with the manner the duct and brake assemblies have been modelled, as the true application would have shrouding within the wheel that distributes the flow more evenly, as mentioned by (FIA Formula 1, 2018), which will significantly change the flow vectors seen as the ducting and shrouds are designed to carefully manage flow within the wheel and brake assemblies. Figure 51 shows the complexity of the geometries employed. Due to the high complexity, and considerable computational resources that would be required to accurately model this in CFD, it was decided not to attempt to represent this type of geometry.

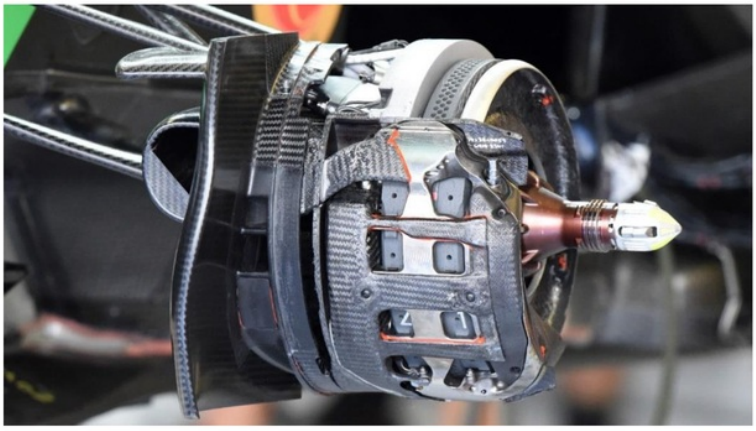


Figure 51 - Force India 2018 Front Brake Assembly (FIA Formula 1, 2018)

The redesign of the flap elements between these designs has also resulted in a significant change in the intensity of the Y250 vortex being generated, as a result of the change in flap tip dimensions and positions.

Figure 52 shows the turbulent regions seen on both designs, with the Y250 vortex on design 1 being of greater intensity and propagating further back through the suspension members. In design 7, the vortex can be seen to be far smaller, and begins to dissipate earlier, leaving less disturbed flow toward the bargeboard areas. The effect of this can be seen in figure 50, where design 7 has significantly higher velocity flow around the edges of the sidepod, where the still energised air is being managed around by the bargeboards, whereas on design 1,

due to the turbulent flow being encountered by the flow management devices, the 'spill' around the sides of the sidepods has far less kinetic energy, and thus lower velocity.

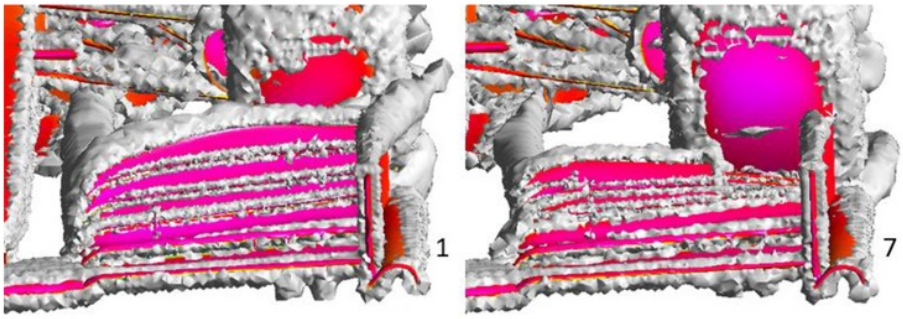


Figure 52 - Y250 Vortex Designs 1 and 7

6.5 Following Car Testing

As previously mentioned, a brief study into the effects of the wake left by a car on the following vehicle has been conducted.

6.5.1 Wake Profile of Single Vehicle

Firstly, the single car geometries can be analysed to see the wake structures left by the vehicles, which will give an indication as to how the wake may affect a following vehicle.

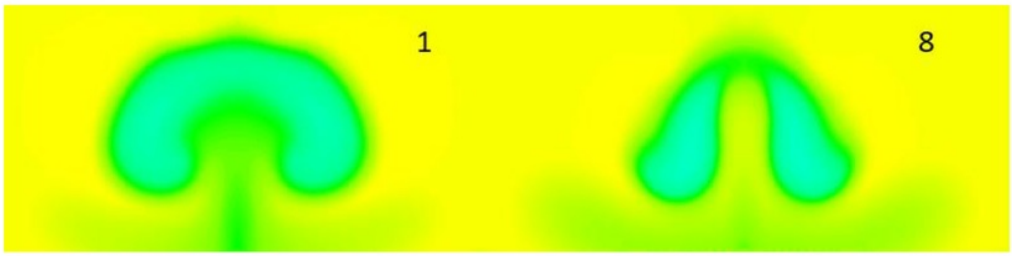


Figure 53 - Vehicle Wake 2.5m behind car designs 1 & 8

When comparing the baseline 2018 and 2019 designs, a significant difference in wake structure can be seen. The 2019 (1) produces a mushroom cloud type wake, where the tip vortices from the rear wing can be seen to have been spread wider apart, with a larger area of the wake, shown by the lower velocity air, higher from the ground plane.

In contrast the 2018 (8) wake is significantly tighter, with the tip vortices remaining closer to the car centreline, and most of the turbulent region much lower to the ground plane. There is also a noticeable increase in the disturbed air at ground level with the 2018 geometry, likely a result of the outwash effects where the flow sent around the vehicle.

These differences can be seen clearly when an Isosurface is applied plotting turbulent kinetic energy.

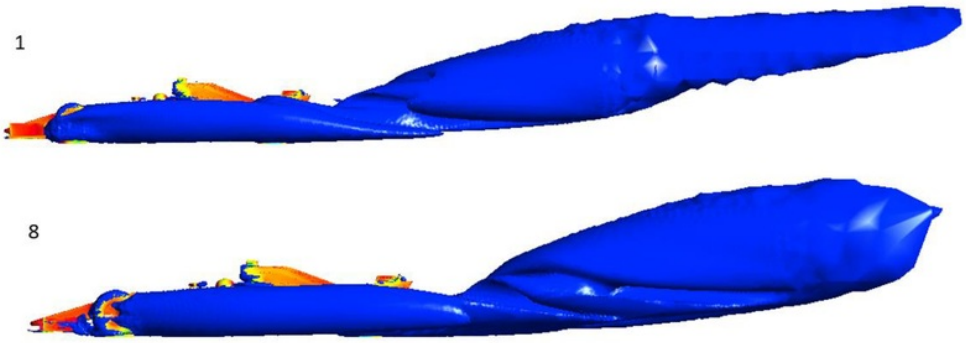


Figure 54 - Isosurface showing wake region designs 1 & 8 Side View

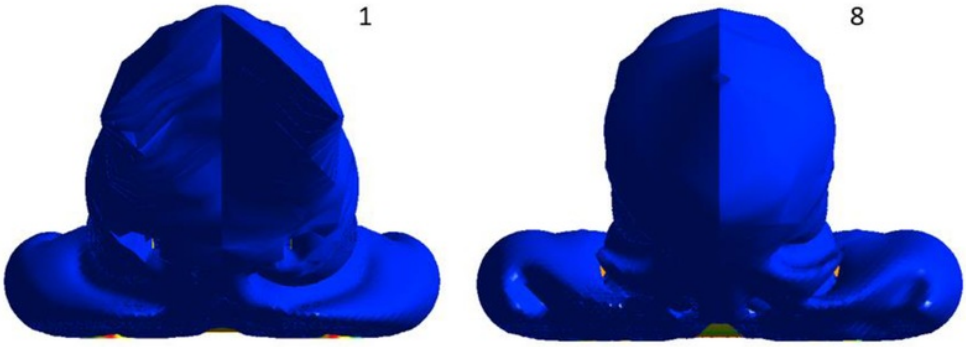


Figure 55 - Isosurface showing wake region designs 1 & 8 Rear view

Figures 54 and 55 demonstrate the significant differences between the wakes produced. As noted, the 2019 wake (1), can be seen to be wider in the section incorporating the rear wing tip vortices, while this section has an upwards trajectory, moving it away from the ground plane. The intensity of the wake can also be seen to deteriorate the further back from the car it moves.

Contrastingly, the wake of the 2018 car follows a much tighter and lower trend, as previously mentioned, while having minimal upwards movement. The difference in wake structures moving down the side of the different designs, generated from the wing and wheel wakes can be seen. The 2019 wake has a slightly higher profile and remains more inboard, where it interacts with the other sections of the car, as previously mentioned. The 2018 wake is wider, due to the outwash produced by the front wing, and slightly lower where the wake is being managed better by the upstream devices.

The structures seen follow a similar trend to those found by (Newbon, et al., 2017), albeit on a geometry resembling an older F1 type car, but with similar trends. Figure 56 shows the comparable wake cross section, where the lower velocity flow sections show very similar

trends to those captured in the data above, giving confidence that the results obtained are representative.

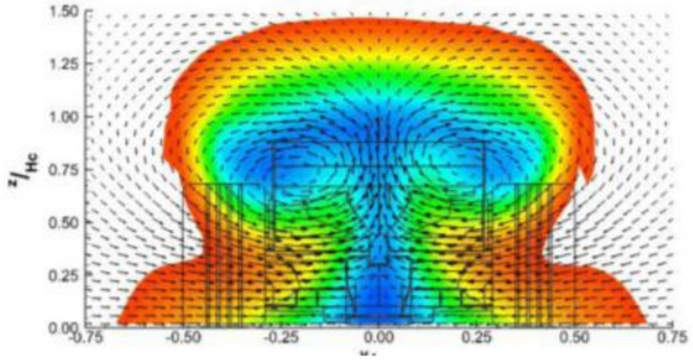


Figure 56 - F1 Car Wake Representation (Newbon, et al., 2017)

When looked at as a horizontal cut plane through the car, 0.25m above the ground plane, a clear difference can be seen between the 2018, 2019 and design 7, shown in figure 57.

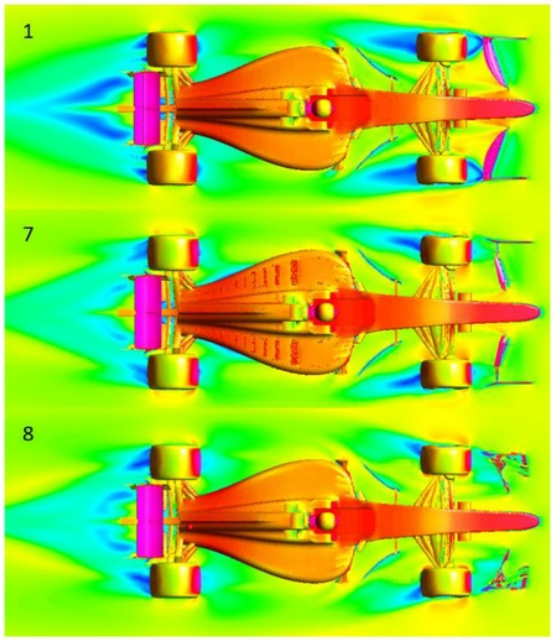


Figure 57 - Vehicle Wake Differences Plane 0.25m above ground

Clear differences can be seen in the trailing wake left behind the vehicle. The wake of the 2019 car shows a far more controlled profile, tapering in heavily to the centreline of the vehicle. It is therefore expected that the wake further rearward of the car will maintain a much narrower path. Due to this more controlled wake, it is expected that the disruption this disturbed air will cause on the following vehicle will be reduced compared to that of designs 7 and 8.

Designs 7 and 8 show a noticeably wider wake region behind the vehicle, which can be seen to be drawn wider by the outwash flow that can be seen moving around the sides of the vehicle compared to design 1. This makes a visible impact on the rear wheel wake, where in designs 7 and 8 the wake draws outboard noticeably, contributing to the wider wake region seen overall, whereas in design 1 the can be seen to draw into the man wake region left by the diffuser and rear wing due to the significant pressure gradient generated by the differing velocity regions seen between the designs. Interestingly, design 7, which closely resembles the design being tested by Alfa Romeo F1 team, bears remarkable similarity to the base spec 2018 flow structures. This shows that it is extremely likely that teams have determined that the outwash characteristic is still most beneficial to the overall performance of the vehicle, given the manner in which it controls airflow back to the downstream components, thus have expended considerable resource on generating designs within the confines of the new rules that allow for a virtually identical flow pattern that was being created the year before.

For comparison, a similar post-processing image, from (Iley Design, 2019) is shown in figure 58.

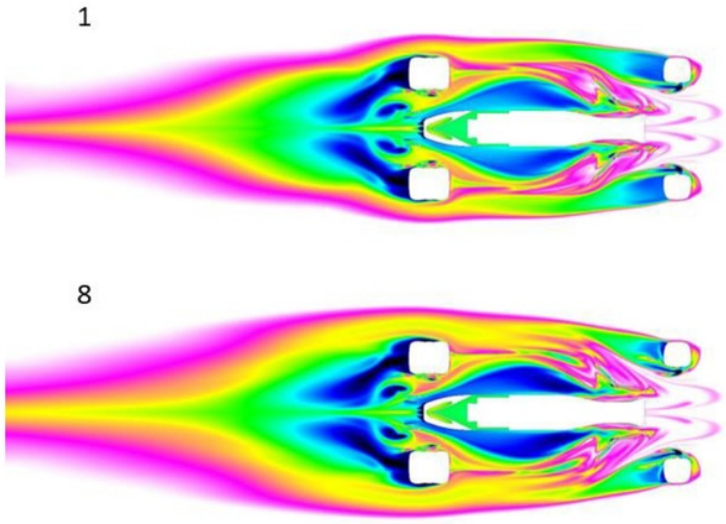


Figure 58 - F1 2018 2019 Wake Comparison (Iley Design, 2019)

While the height above ground that this cut plane has been positioned is not known, therefore direct comparison cannot really be made, the trends seen in the differing images are useful. The above images have been labelled in accordance with the design concept labels used throughout this report.

As shown, the wake of the 2018 car (8), follows a wider path downstream of the vehicle compared to the 2019 car (1), with the outwash from the front wing clearly visible and

drawing the front wheel wake outboard noticeably. The intensity of the low velocity zone in the front wheel wake is also significantly smaller than that seen from the 2019 car (1). When compared with the results shown in figure 57, these trends both follow closely, with excellent similarity seen in the front wheel wake regions as well as the complete vehicle wake, giving credence to the validity of the results obtained from the CFD testing.

6.5.2 Following Car CFD Testing

Figure 59 shows the CAD produced for the following car CFD testing, where the following vehicle has been set 5 car lengths behind the lead car, which equates to approximately 0.65s separation at the tested velocity (40 m/s).



Figure 59 - Following Car CFD Testing Geometry 2019 Spec Cars

The testing was conducted using the 2018 and 2019 base specification cars to characterise the difference in concept influence on following car, as well as design 7 due to it being the most aggressive of the tested design concepts.

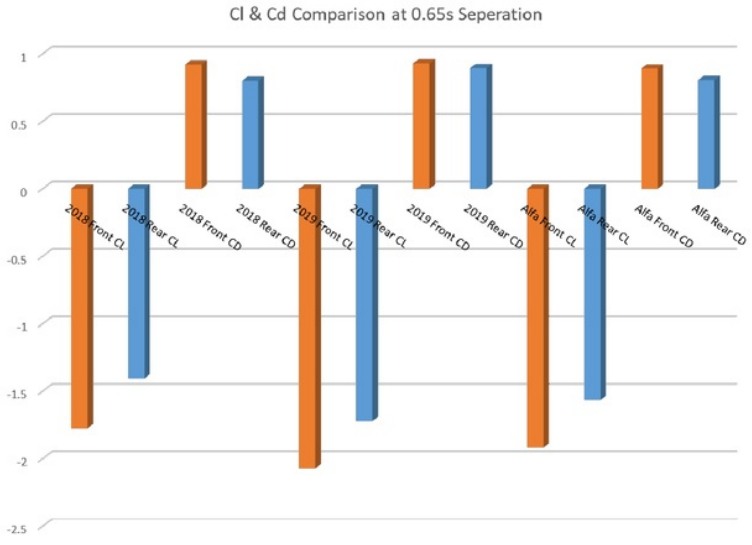


Figure 60 - Cl and Cd results from 5 Car Length Separation Testing

Figure 60 shows the Cl and Cd values found from the testing. As expected, a drop in both Cl and Cd was seen on the following car for all designs, with varying levels of reduction. These results are highlighted more clearly in figures 61 and 62 when viewed as percentages, compared to the 2018 base specification (8).

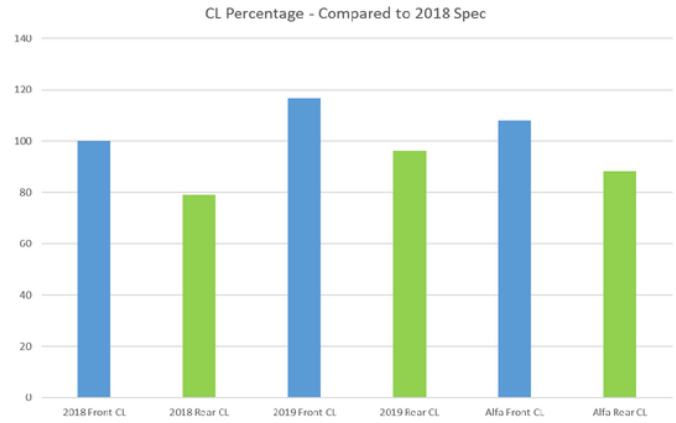


Figure 61 - Following Car Testing Cl Percentage Values

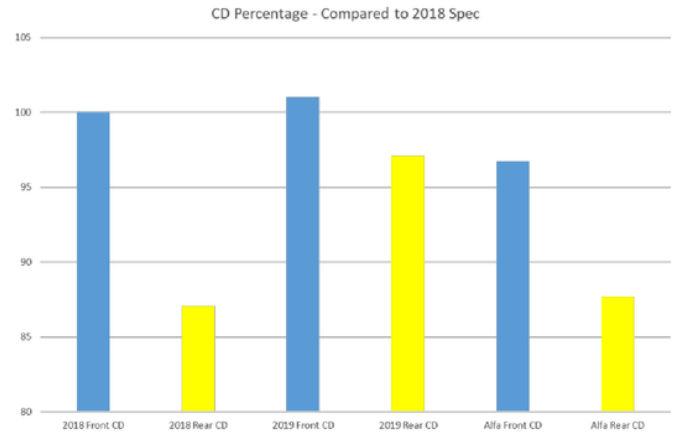


Figure 62 - Following Car Testing Cd Percentage Values

Figure 61 clearly shows the higher Cl values generated by both 2019 designs (negative Cl) over the baseline 2018 design for the front car. The reduction on design 1 is 16.9% and design 7 experiences an 18.3% reduction for the following car. Contrastingly, the 2018 design (8) experiences a 20.9% reduction on the following car.

Given the comparison of wake structures between these designs, carried out previously, the results do follow the anticipated trend. The more controlled wake of design 1 has resulted in less of an impact on the following car, while the 2018 design, with its pronounced outwash characteristics and large, lower wake signature has produced the largest reduction. Design 7, which produced a wake that bore a strong similarity to the 2018 wake, yielded reductions

that were somewhere between the two designs. Given the visible wake structures, these results are logical, and give confidence in the CFD and its ability to model two separate vehicles in the same domain.

A similar trend is seen with the Cd values, where the 2018 design experienced a 13% reduction, the 2019 only a 3.9% reduction and design 7 a 9.4% reduction. Given the wider wake field generated by the 2018 design, it is logical that the disturbed, lower energy flow will be contacting a larger area of the following car, thus allowing a greater reduction in drag due to the lower levels of stagnation and skin friction seen, especially on the front wing of the following car, where (Newbon, et al., 2017) states the largest effect of operating in a wake is seen. As an opposite, the 2019 design, with its tighter wake, has less influence in this way, and more of the following car will be exposed to flow that is closer to the higher energy freestream the lead car sees, resulting in less of a drag reduction, as per (Smith, 2013). This type of effect, where a body is encountering the disturbed wake from an upstream body is well documented in the cycling world, where the drag reduction is well documented, as per (Blocken, et al., 2013) and (Blocken, et al., 2018).

To more clearly visualise these differences, a cut pane 0.3m above ground has been added showing the velocity contours seen from the CFD testing, for designs 1 and 8. It should be noted that the scaling has been changed to between 0-45 m/s to highlight the velocity gradients better.

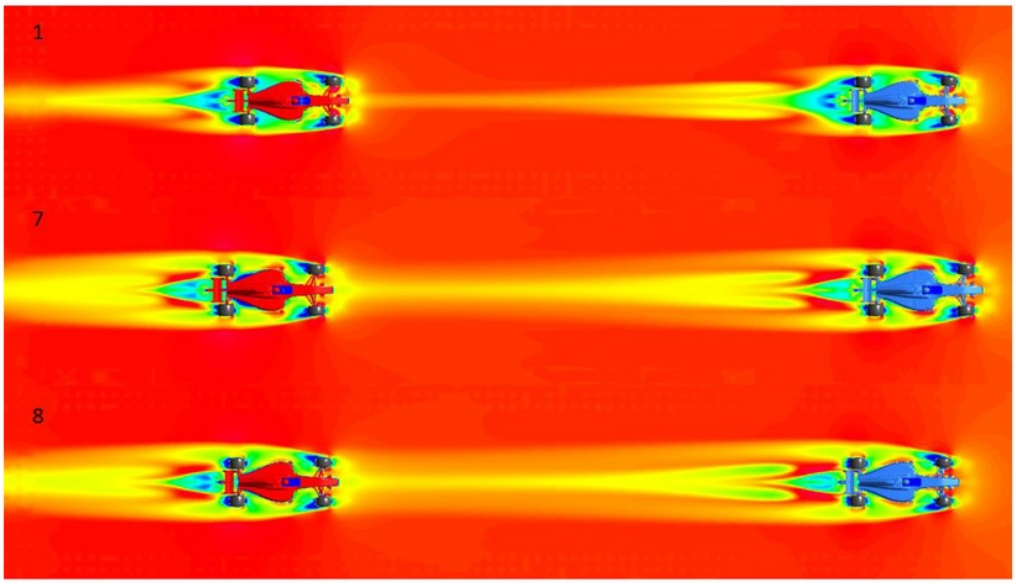


Figure 63 - Following Car Testing Velocity Contours

The width of the wake by the time it contacts the following vehicle can now clearly be seen, and follows the described trends above, as well as correlating to the reductions in Cl and Cd

values seen. The 2019 front wing, with its lack of outwash results in a very narrow wake, likely contributing to the better performance of the following car of the same specification. The 2018 wake pattern is significantly wider, essentially encompassing the whole front wing of the following car, with design 7 being closer to design 8 (2018), although not as wide of a wake signature.

Another study was conducted, in the same manner, but with a separation distance equating to 0.35 seconds between cars, to evaluate the impact of operating within the near-wake region of another vehicle. It should be noted that, due to geometric issues and meshing problems, the 2018 base spec run was conducted with a polyhedral mesh type instead of tetrahedral, as such the exact numbers can only be considered representative and not directly comparable as this change will have affected the CFD solver solution.

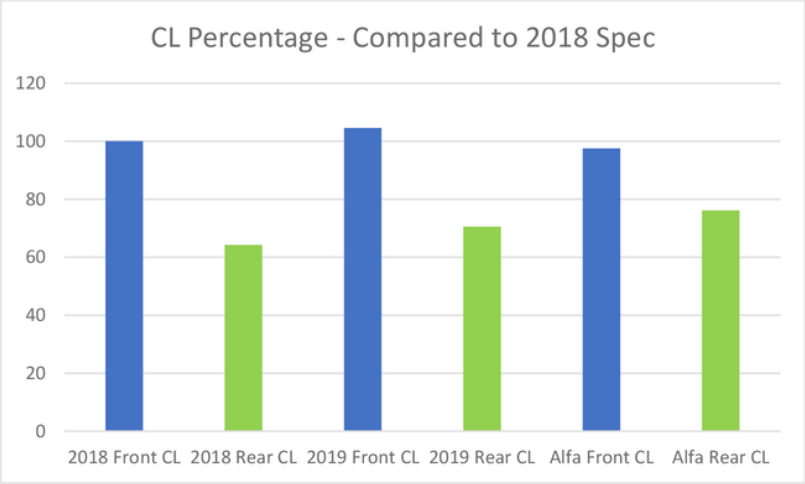


Figure 64 - Following Car Cl Results 0.35s Separation

The Cl changes, shown in figure 64, follow a similar trend to those seen at the 0.65s separation, however a noticeably larger drop in Cl can be seen on all designs, with up to 36% losses seen on the 2018 design. This drop follows what wold be expected, given that (Azmi, et al., 2017) explain how the near-wake region, with heavily turbulent flows will have significantly impact following vehicles due to the lack of clean, energised onset flow available. Interestingly, despite having a similar wake signature to the 2018 design, the Alfa Romeo styled design suffered significantly less of a drop on the following car, only 21% compared to the 36% for the 2018 and 34% for the 2019 designs. Since the wake structure was like the 2018, it can be assumed that the reduced impact is not a result of the wake management but coming from the differing front wing designs.
Without further study, it cannot be fully defined, but it would appear from these results that the significantly more simplified front wing of the Alfa Romeo style design (7) is far less

susceptible to performance degradation from operating in turbulent flows, certainly when compared to the 2018 style design. This design sensitivity should be accounted for across all results detailed above, in that it cannot be said that the wake signature is the sole reason for the differing levels of change seen, given the front wing design will be having a notable influence as well.

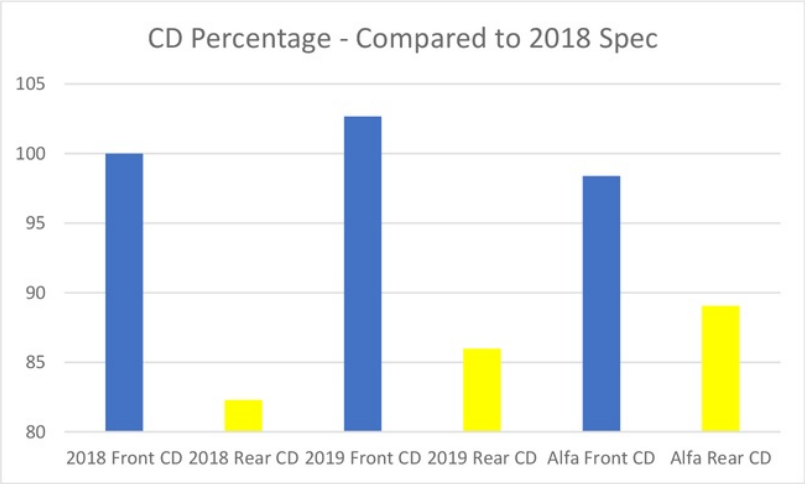


Figure 65 - Following Car Cd Results 0.35s Separation

In contrast to the data seen at 0.65s separation, the 2019 design saw a far more significant reduction in Cd value when in the near-wake region. Given that the wake of this design was far narrower at the 0.65s, it is understandable why there was less of a drag reduction. However, at 0.35s separation, the following car is now operating in a much wider section of the wake, hence the greater reduction in drag. This is further highlighted when looking at an Isosurface of the turbulent kinetic energy, which shows the wide spread of turbulence encountered by the following cars front wing, shown in figure 66.

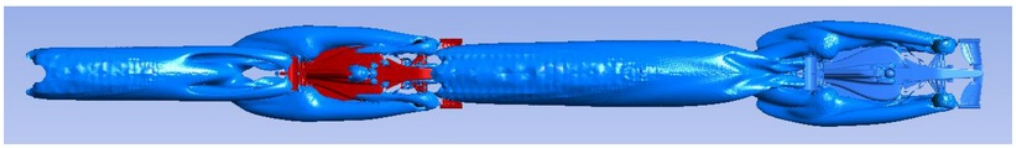


Figure 66 - 2019 Specification Following Car Isosurface

The other designs followed a similar trend to before, as was expected given the overall wider wake signatures seen with these designs.

7.0 Conclusion & Evaluation

Regarding the validations works conducted in the early stages of the project have highlighted the limitations of attempting to use Design of Experiment software in the context of computational fluid dynamics. Given the failure of Design Expert 11 to predict, with any real degree of accuracy, the required settings to validate a known CFD case against reference data, it can be said that this methodology should not be applied in cases of external aerodynamics. However, it is not true to say that this investigation has ruled that DOE software is incapable of being used in a CFD context, as there are many other programmes available that may be more capable than the one tested and could have yielded more positive results.

A good characterisation of the wake structure generated by a rotating exposed wheel has been achieved by the investigation. In a CFD environment it has been proven that modelling the wheels as rotating items is the only way to achieve a wake signature that correlates to other published works by (Axereo-Cilies & Iaccarino, 2012) and (Croner, et al., 2013). Once modelled in this way, the generation and propagation of the wake structure has been captured with good accuracy, allowing for representative analysis to be conducted.

The impact of locally sited components on the wake generated by the front wheel, in this case namely the brake duct assembly, can be said to be of less significance than was expected. Given the geometries tested, which were of a relatively basic design, the results obtained do give enough data to say this with certainty, especially when looking at the influence of front brake duct design on Formula 1 cars of recent years, according to (FIA Formula 1, 2018). When testing the geometries that represented the flow rejection slots as well as the reduced orifice dimensions, it was clearly found that the change in flow structures, with the resulting areas of separation and turbulence, in all cases gave worse Cl and Cd figures, with a minimal impact of the overall flow structures seen around the whole assembly. On this basis, the works conducted have shown there is no benefit to be gained by altering a brake duct in the ways tested in this investigation, and that flow conditioning to manipulate wheel wake should be done using upstream devices.

The investigation into front wing design has shown that the concept of generating more outwash, to direct onset flow outboard of the front wheel. The influence that this causes on the front wheel wake has been proven to be beneficial to the overall aerodynamic performance of the vehicle. This appears to be a result of the wake region being drawn outboard, and thus reducing its interaction with the downstream devices on the vehicle.

However, the results have clearly shown that the design of the upper flap elements of the front wing can have significant influence over the downstream devices, most noticeably the working of the floor and diffuser areas of the car. Due to this finding, careful consideration should be given to the way the wing is designed, not only for control of the front wheel wake, but also to manage the impact the changes in upwash and flow direction have on the other aerodynamic devices. Additionally, testing has proven that manipulation of the Y250 vortex propagating from the front wing is difficult to control from the wing design alone. Looking at the post-processing results, it seems more likely that any control of the Y250 vortex would be best achieved using flow conditioning devices mounted to the underside of the cockpit section, or by design of the barge board devices.

The intent of the new 2019 regulations within Formula 1 had the intent of reducing the wake signature of vehicles, with the assumption that this would help improve a cars ability to follow, as per (FIA Formula 1, 2018). The testing with the following car geometries has shown that, with the differing design philosophies that have been demonstrated by the teams, all of which are within the regulatory design constraints, the impact on the following car is still very similar to that seen with the 2018 specification cars, albeit with more overall downforce, but still seeing similar levels of drop-off. It can be said that the new regulations, had the cars been designed as the working group in F1 intended as design 1, the impact of wake would have been greatly reduced and overtaking would likely have improved. However, the testing has shown that the design philosophies followed by the current 2019 cars has resulted in wake structures and management techniques that very closely mimic those of the original 2018 designs they replaced. As a result, it is expected that the ability to follow in a wake, and therefore to see improved overtaking, will improve, due to the slightly reduced drop-off seen and overall higher downforce produced, but it is unlikely to be the considerable improvement originally intended. This is supported by an article from (SkySports.com, 2019) where the overtaking situation at the 2019 Melbourne Grand Prix was improved over last year, although not conclusive.

8.0 Recommended Further Works

Ideally, if the resource had been available, it would have been preferable to have conducted a deeper study, involving differing pieces of software, into the true capabilities of DOE when applied to CFD validation studies. As previously mentioned, the works conducted cannot say definitively that this approach would not work, and this area would require deeper study as it is felt based on previous use, the DOE should yield excellent time savings.

It has already been stated that the investigation into the brake duct as a flow conditioning device yielded poor results, however the limitations of the features studied do not draw a complete picture of the potential benefits that could be made in this area. It would be desired to conduct more detailed testing, using geometries that involve externally mounted, or fully integrated flow conditioning devices, such as turning vanes, on the brake ducts, to correctly map the potential impacts that can be made. In a similar manner, it is believed that considerable influence could be gained by manipulation of the geometry of the suspension members, which is an area that has been neglected in these works.

The F1 geometry used (Perrinn, 2017), while representative, is not an accurate reflection of the geometry for the 2019 style wings. Given that (FIA, 2018) and (FIA Formula 1, 2018) clearly define there are significant changes to the barge boards and rear wing assemblies, which are areas that have been identified in this report as having a significant influence on the trailing wake left by the vehicle, it would be preferable to have conducted the 2019 studies using a more representative geometry. The reason for not doing so in the main investigation was so that comparative change could be monitored, effectively isolating the influence of the front wing designs alone, ignoring the rest of the geometry, although it was known this would not give a full indication of the true performance of the 2019 designs. Additionally, no investigation or consideration has been given to the influence of roll, pitch and yaw on the performance of any of the designs, which could form the basis for additional study.

Works Cited

Ahmad, N., Abo-Serie, E. & Gaylard, A., 2010. *Mesh Optimisation for ground vehicle Aerodynamics,* Coventry: CFD Letters.

Ahmad, S., Ramm, G. & Faitin, G., 1984. Som Salient Features of the Time-Averaged Ground Vehicle Wake. *SAE,* Volume 569, pp. 1-30.

Airbus, 2014. *How to Properly Operate the Carbon Brakes?,* s.l.: Airbus.

Alahmer, A. & Al-Dabbas, M., 2014. Modelling ad Simulation Study to Predict the Cement Portland Cyclone Seperation Perofrmance. *Emirates Journal for Engineering Research,* 19(1), pp. 19-25.

Axereo-Cilies, J. & Iaccarino, G., 2012. An Aerodynamic Investigation of an Isolated Rotating F1 Wheel Assembly. *Journal of Fluids Engineering,* 134(12), pp. 101-121.

Azmi, A. et al., 2017. *Study of Airflow Characteristics of F1 Car,* s.l.: IOP Publishing.

Bakker, A., 2006. *Meshing - Applied Computational Fluid Dynamics.* [Online]
Available at: http://www.bakker.org/dartmouth06/engs150/07-mesh.pdf
[Accessed 15 10 2018].

Barnard, H., 2001. *Road Vehicle Aerodynmaic Design.* 2nd ed. St Albans: Mechaero Publishing.

Bathe, K.-J. & Zhang, H., 2009. A mesh adaptivity procedure for CFD and fluid-structure interactions. *Computers & Structures,* , 87(), pp. 604-617.

Bernstein, S. & Joppa, R. G., 1976. Development of minimum correction wind tunnels. *Journal of Aircraft,* , 13(4), pp. 243-247.

Blocken, B. et al., 2013. CFD Simulations of the Aerodynamic Drag of two Drafting Cyclists. *Computers and Fluids,* Volume 71, pp. 435-445.

Blocken, B., Toparlar, Y., van Drueren, T. & Andrianne, T., 2018. Aerodynamic Drag in Cycling Team Time Trials. *Journal of Wind Engineering and Industrial Aerodynamics,* 182(182), pp. 128-145.

CFD Online, 2014. *Ahmed Body.* [Online]
Available at: https://www.cfd-online.com/Wiki/Ahmed_body
[Accessed 15 10 2018].

Collins, L. M., Dziak, J. J. & Li, R., 2009. Design of Experiments with Multiple Independent Variables: A Resource Management Perspective on Complete and Reduced Factorial Designs. *Psychological Methods,* 14(3), pp. 202-224.

Croner, E., Bezard, H., Sicot, C. & Mothay, G., 2013. Aerodynamic Characterisation of the Wake of an Isolated Rolling Wheel. *International Journal of Heat and Fluid Flow,* Volume 43, pp. 233-243.

Diasinos, S., Barber, T. & Doig, G., 2015. The Effects of Simplifactions on Isolated Wheel Aerodynamics. *Journal of Wind Engineering and Industrial Aerodynmaics,* Volume 146, pp. 90-101.

Diasinos, S., Barber, T. & Doig, G., 2015. The effects of simplifications on isolated wheel aerodynmaics. *Journal of Wind Engineering and Aerodynamics,* Volume 146, pp. 90-101.

Diasinos, S. & Gatto, A., 2008. Experimental Investigation into Wing Span and Angle of Attack Effects on sub-scale Racing Car Wing/Wheel Interactions. *Experimental Fluids,* Volume 45, pp. 537-546.

Doodle, F., 2018. *Formula 1 2018 Style Front Wing,* s.l.: GrabCAD.

F1Technical.net, 2018. *Mercedes AMG F1 W08 EQ Power+.* [Online]
Available at: https://www.f1technical.net/forum/viewtopic.php?t=25964&start=930
[Accessed 18 03 2019].

Federation International de l'Autombile, 2018. *Formula 1 Techncal Regulations 2018.* 3rd ed. s.l.:FIA.

FIA Formula 1, 2018. *Aero Changes for 2019 to Promote Overtaking.* [Online]
Available at: https://www.formula1.com/en/latest/article.aero-changes-to-promote-overtaking-approved-for-2019.153os6PCPsl0SaQSsE0cQ6.html
[Accessed 10 03 2019].

FIA Formula 1, 2018. *Teams trial 2019 Spec Wings.* [Online]
Available at: https://www.formula1.com/en/latest/article.teams-trial-2019-spec-front-wings-in-testing.2RHNhtpjk4sU8kiQ6SAWU6.html
[Accessed 18 03 2019].

FIA Formula 1, 2018. *Understanding F1 Racing - Brakes.* [Online]
Available at: https://www.formula1.com/en/championship/inside-f1/understanding-f1-racing/Brakes.html
[Accessed 21 03 2019].

FIA Formula 2, 2017. *Formula 2 2017 Multimedia.* [Online]
Available at:
http://www.fiaformula2.com/Multimedia/Photos/?tags=1220&gpid=8424&showall=true
[Accessed 05 11 2018].

FIA, 2018. *Formula 1 Technical Regulations 2019.* 2nd ed. s.l.:FIA.

Field, A. P. & Hole, G., 2003. *How to Design and Report Experiments.* London: SAGE.

Formula One World Championship Ltd, 2018. *F1 Brakes.* [Online]
Available at: https://www.formula1.com/en/championship/inside-f1/understanding-f1-racing/Brakes.html
[Accessed 05 11 2018].

Formula1.com, 2018. *Drag Reduction System.* [Online]
Available at: https://www.formula1.com/en/championship/inside-f1/rules-regs/Drag_Reduction_System.html
[Accessed 01 10 2018].
Govender, V. & Barton, D., 2009. *Multibody System Simulation and Optimisation of the Driving Dynamics of a Formula SAE Race Car,* Warrendale: SAE International.
Guilmineau, E. et al., 2017. *Assessment of Hybrid RANS-LES Formulations for Flow Simulation around the Ahmed Body,* s.l.: Elsevier.
Hetawal, S., Gophane, M., Ajay, B. & Mukkamala, Y., 2014. Aerodynmaic Study of Formula SAE Car. *Procedia Engineering,* Volume 97, pp. 1198-1207.
Houghton, E., Carpenter, P. W., Collicott, S. H. & Valentine, D. T., 2013. *Viscous Flow and Boundary Layers.* [Online]
Available at: https://sciencedirect.com/science/article/pii/b9780080966328000084
[Accessed 17 3 2019].
Houghton, E. & Carpenter, R., 2003. *Aerodynmaics for Engineering Students.* 5th ed. Oxford: Butterworth-Heinemann.
Iley Design, 2019. *Integrated Engineering Solutions,* s.l.: Iley Design.
Issakhanian, E., Elkins, C., Lo, K. & Eaton, J., 2010. An Experimental Study of Flow Around a Formula 1 Tyre. *Journal of Fluid Engineering,* 132(1), pp. 1-8.
Jamei, S. et al., 2016. Design Parametric Study of a Compound Wing-in-Ground Effect. II: Aerodynamics Coefficients. *Journal of Aerospace Engineering,* , 29(1), p. 04015023.
Kajiwara, S., 2017. Passive Variable Rear Wing Aerodynamics of an Open-Wheel Racing Car. *Automotive & Engine Technology,* 2(1), pp. 107-117.
Katz, J., 1995. *Race Car Aerodynamics: Designing for speed.* Cambridge: Bentley.
Klinzing, W. P. & Sparrow, E. M., 2009. Evaluation of turbulence models for external flows. *Numerical Heat Transfer Part A-applications,* , 55(3), pp. 205-228.
Lanfrit, M., 2005. *Best Practie guidelines for handling Automotive Aerodynamics with FLUENT,* Birkenweg: Fluent Deutshland GmbH.
Lee, K., 1999. *Principals of CAD/CAM/CAE Systems.* Harlow: Addison-Wesley.
MaxF1.net, 2019. *Technical Analysis Mercedes F1 2019 W10 EQ Power+.* [Online]
Available at: https://maxf1.net/en/technical-analysis-2019-f1-mercedes-f1-w10-eq-power/
[Accessed 19 03 2019].
Medes-Alves, R. & de Almeaida, O., 2017. Validation of Experimental & Numerical Techniques for Flow Analysis over an Ahmed Body. *International Journal of Engineering Research & Applications,* 7(4), pp. 63-71.
Meile, W. et al., 2010. Experiments and numberical simulations of Aerodynamics around Ahmed bodies. *CFD Letters,* 3(1).

Motorsport Association, 2018. *MSA Yearbook 2018.* 62nd ed. London: JLT.

Motorsport.com, 2016. *Merceds Development: Front Wing and Brake Duct.* [Online]
Available at: https://www.motorsport.com/f1/news/bite-size-tech-mercedes-development-front-wing-and-brake-duct-844121/844121/
[Accessed 10 03 2019].

NASA, 2009. *Navier-Stokes Equations.* [Online]
Available at: https://www.simscale.com/docs/content/simwiki/cfd/whatiscfd.html
[Accessed 10 03 2019].

NASA, 2016. *CFD Verification & Validation.* [Online]
Available at: https://www.grc.nasa.gov/www/wind/valid/tutorial/overview.html
[Accessed 14 10 2018].

Newbon, J., Sims-Williams, D. & Dominy, R., 2017. Aerodynamic Analysis of Grand-Prix Cars Operating in Wake Flow. *SAE International Journal of Passenger Cars,* 10(1), pp. 318-329.

Oulton, R., 1971. *AIRCRAFT WITH COMPOUND WING.* [Online]
Available at: http://freepatentsonline.com/3776491.html
[Accessed 20 3 2019].

Perrinn, N., 2017. *Opensource F1 Car CAD Model,* s.l.: Perrinn Ltd.

Petr, 2018. *Formula 1 2019 Style Wing,* s.l.: GrabCAD.

Rapp, B., 2017. *Microfluids: Modelling, Mechanics and Mathematics.* 1st ed. Cambridge: Elsevier.

Renz, R., Seifert, G. & Krenkel, W., 2012. Intergration of CMC Brake Discs in Automotvie Applications. *Inernational Journal of Applied Cermaic Technology,* 9(4), pp. 712-724.

Rezaeiha, A. et al., 2018. Towards accurate CFD simulations of vertical axis wind turbines at different tip speed ratios and solidities : guidelines for azimuthal increment, domain size and convergence. *Energy Conversion and Management,* , 156(), pp. 301-316.

Saddington, A., Knowles, R. & Knowles, K., 2007. Laser Doppler Anemometry Measurements in the Near-Wake of an Isolated Formula 1 Wheel. *Experimental Fluids,* Volume 42, pp. 671-681.

Simscale, 2016. *What is CFD.* [Online]
Available at: https://www.simscale.com/docs/content/simwiki/cfd/whatiscfd.html
[Accessed 10 03 2019].

SkySports.com, 2019. *F1 2019 - Ross Brawn Encouraged by Overtaking following Aero Changes.* [Online]
Available at: https://www.skysports.com/f1/news/12433/11670725/f1-2019-ross-brawn-encouraged-by-overtaking-following-aero-changes
[Accessed 01 04 2019].

Smith, C., 1978. *Tune to Win.* California: Aero Publishers.
Smith, J., 2013. *Fundamentals of Motorsport Engineering.* Cheltenham: Nelson Thornes.
Som, S., Senecal, P. & Pomraning, E., 2012. *Comparison of RANS and LES Turbulence Models against constant volume Diesel Experiments,* San Antonio: ILASS America.
Tunay, T., Sahin, B. & Ozbolat, V., 2014. Effects of rear slant angles on the flow characteristics of Ahmed body. *Experimental Thermal and Fluid Science,* , 57(), pp. 165-176.
Versteeg, W. & Malalasekera, W., 2007. *An Introduction to Computational Fluid Dynamics.* 2nd ed. Harlow: Pearson Prentice Hall.
Wenjun, G., Nelias, D., Lyu, Y. & Liu, Z., 2018. Numerical Investigation of Flow around a Clyinder with Two Free Ends. *Ocean Engineering,* Volume 156, pp. 373-380.
Wiley, R. H., 2009. Trade-offs in the design of experiments.. *Journal of Comparative Psychology,* 123(4), pp. 447-449.
Worldpress.com, 2013. *Formula 1 Car Vortices.* [Online]
Available at: https://tianyizf1.wordpress.com/tag/y250-vortex/
[Accessed 19 03 2019].
Wright, P., 2001. *Formula 1 Technology.* Warrendale: Society of Automotive Engineers.
Yares, E., 2012. *Optimising the Design of an F1 Brake Duct.* [Online]
Available at: https://www.designworldonline.com/optimizing-the-design-of-an-f1-brake-cooling-duct/
[Accessed 14 03 2019].
Yokozeki, e. a., 2006. Mechanical Properties of corrugated composites for candidate material of flexible wing structures. *Composites Part A,* 37(10), pp. 1578-1586.

Appendix A

A.1 Thermal Management Issues

Exact information on operating temperatures of the friction material/disc surface in racing applications is somewhat limited. Due to the proprietary nature of the brake systems in use, manufacturers do not give out much information.
Vague information regarding the materials and operating temperatures is available from (Formula One World Championship Ltd, 2018), which describes the material for the disc as carbon composite, reaching peak temperatures of up to 1200 degrees Celsius.
Unfortunately, there is little information available regarding carbon discs, more literature can be found regarding carbon ceramic discs which are more commonly used for performance road vehicles, unlike carbon only discs. (Renz, et al., 2012) describes that ceramic brake systems are used on road vehicles as the temperature requirements are lower, wear rates significantly better than carbon and the driver feel/feedback through the pedal is improved in low temperature operation, unlike carbon systems.

One area where carbon/carbon brake systems are in use heavily is the aviation industry. It is very common for modern large body airliners to use multiplate carbon brake stacks in the landing gear systems to provide braking. Temperature ranges are more available for these applications, although these will clearly differ from the racing vehicle applications.
It would seen that, depending on the application, for an airliner the expected operating temperature at the disc would be between 550-750 degrees during a braking event on landing as shown in figure 3.
Further testing will be conducted using the BPS 4.8 Simulator available on site to obtain brake temperature information based on simulated racing laps using a suitably representative vehicle model.

A.2 Simulator Brake Temperature Testing

Using the BPS 4.8 Driver in the loop simulator, a series of circuit lap tests were conducted using the Dallara GP2/11 vehicle model around Silverstone GP circuit.
The vehicle model was constructed by Carlin Motorsport and used for driver training, as such can be considered representative to the operational characteristics of the vehicle.
The coding within the software models changes the way in which the brake temperatures are modelled using a brake duct setting. This is done with a scaling factor, “Brake cooling rate

per brake duct setting" of 0.79*10^-4 per setting increment. The GP2/11 model has a range of 10 brake duct setting, 1-10.

The model is set with an optimal brake temperature of 525 Celsius, with brake fade occurring 125 Celsius above or below this optimum temperature.

Circuit testing was conducted for the default setting (5), minimum setting (1) and maximum setting (10). Results shown below.

DUCT SIZE	PEAK TEMP	MIN TEMP	VMAX	LAP TIME
MIN	899.5	360.1	287.5	1.40.065
MID	639.2	128.5	287.4	1.39.074
MAX	468.8	72.2	287.8	1.40.547

The data shows that there is significant differences in temperature obtained when the duct settings are altered. With the duct settings at minimum the peak temperatures seen in heavy braking zones are 260 degrees higher than the default duct setting.

Given that there is only a 125 degrees window around the optimum temperature of 525, the minimum and maximum settings for the duct result in temperatures in the fade region, which results in a reduction in braking torque. There is no information on the reduction in torque that the physics engine applies during fade.

Vmax of the vehicle is unaffected by brake duct setting, meaning that, as expected, there is no drag coefficient change for duct settings. This means and change in drag coefficient will have to be input into the aerodynamic coding for each testing run.

Lap times are affected by the duct settings as expected, in that the runs conducted where the brakes are operating in the fade region yielded slower lap times than when they were operating optimally.